



HAL
open science

Earliest life on Earth: Evidence from the Barberton Greenstone Belt, South Africa

Martin Homann

► **To cite this version:**

Martin Homann. Earliest life on Earth: Evidence from the Barberton Greenstone Belt, South Africa. Earth-Science Reviews, 2019, 196, 10.1016/j.earscirev.2019.102888 . hal-02933520

HAL Id: hal-02933520

<https://hal.univ-brest.fr/hal-02933520>

Submitted on 8 Sep 2020

HAL is a multi-disciplinary open access archive for the deposit and dissemination of scientific research documents, whether they are published or not. The documents may come from teaching and research institutions in France or abroad, or from public or private research centers.

L'archive ouverte pluridisciplinaire **HAL**, est destinée au dépôt et à la diffusion de documents scientifiques de niveau recherche, publiés ou non, émanant des établissements d'enseignement et de recherche français ou étrangers, des laboratoires publics ou privés.

Earliest life on Earth: Evidence from the Barberton Greenstone Belt, South Africa

Martin Homann¹

¹European Institute for Marine Studies, CNRS-UMR6538 Laboratoire Géosciences Océan, Technopôle Brest-Iroise, 29280 Plouzané, France. *corresponding author: martin.homann@univ-brest.fr

Studies investigating the structure and diversity of Earth’s record of life older than 3.2 Ga are restricted to two locations worldwide in which sedimentary rocks have escaped regional high-grade metamorphism and penetrative deformation: the Pilbara Craton of Western Australia and the Barberton Greenstone Belt (BGB) in the Kaapvaal Craton of South Africa. This paper provides a South African perspective on the evidence of Paleoproterozoic life; a record that is often overlooked in the literature. It aims to summarize and critically review previously reported claims of early life in the BGB, gives an overview of the latest findings, and provides an outlook on potential future discoveries.

The ~15 km thick, volcanic-sedimentary succession making up the Barberton Supergroup was deposited between 3.55 to ca. 3.20 Ga and can be subdivided in three stratigraphic units that provide a unique window into a diverse and widespread Paleoproterozoic microbial ecosystem landscape. Putative biosignatures occur almost throughout the entire BGB stratigraphy and range from carbonaceous cherts containing filamentous, spheroidal, and lenticular microstructures, traces of hydrothermal biofilms, photosynthetic microbial mats, remnants of pseudocolumnar stromatolites, and large, organic-walled spheroidal microfossils of currently unknown affinity. The BGB also contains one of the world's oldest known record of tufted microbial mats, which extensively colonized tidally-influenced, siliciclastic shorelines and were most likely formed by filamentous photosynthesizers. Other mat-associated biosignatures include silicified gas bubbles, domes and lenses that likely formed due to metabolic activity or the decay of buried organic matter. Some of these subsurface voids beneath the cohesive mats were inhabited by the earliest known forms of cavity-dwelling microbial communities that were probably dominated by chemotrophic or photosynthetic microbes. Recently discovered terrestrial microbial mats, once thriving in a fluvial-dominated setting, represent the oldest macroscopically-visible fossil traces of life on land, which is also supported by the occurrence of nearby paleosols that carry signals of biogenic sulfur fractionation.

The wealth of preserved microbial biosignatures from marine, fluvial, hydrothermal, and possibly planktonic settings combined with the high spatial and temporal resolution of the Barberton Greenstone Belt deposits is truly exceptional, consequently the BGB deserves an equal level of attention and protection for future generations like its Australian counterpart.

57
58
59
60
61
62
63
64
65
66
67
68
69
70
71
72
73
74
75
76
77
78
79
80
81
82
83
84
85
86
87
88
89
90
91
92
93
94
95
96
97
98
99
100
101
102
103
104
105
106
107
108
109
110
111
112

36
37
38
39
40
41
42
43
44
45
46
47
48
49
50
51
52
53
54
55
56
57
58
59
60
61
62
63
64
65
66
67
68
69

1. Introduction

The Archean rock record is sparse, largely metamorphosed, and preserved in fragmented Greenstone Belts, which occur wedged in between plutonic and metamorphic rocks in the cratonic lithosphere of nearly all continents. However, only the Barberton Greenstone Belt (BGB) of South Africa and Swaziland and the contemporaneous Pilbara Greenstone Belts (PGBs) of Western Australia contain well-preserved sedimentary rocks of Paleoproterozoic age (>3.2 Ga), which experienced only greenschist facies metamorphism and relatively minor deformation. With an areal extent of ~ 6000 km² and an age of ~ 3.55 – 3.20 Ga the BGB is significantly smaller and captures a slightly shorter time interval in comparison to the PGBs (~ 60000 km², ~ 3.52 – 2.94 Ga), however, the deposits preserved in the BGB are characterized by often laterally consistent outcrops with correlatable facies, a generally better exposure, and very good accessibility. Lithified aquatic sediments in both of these volcano-sedimentary “enclaves” are considered the most suitable archive of ancient microbial life, as water is one of the fundamental requirements for life. Consequently, the sedimentary deposits have been extensively studied for traces of early life in these two localities and the reported findings have been critically reviewed especially for the Pilbara Greenstone Belts, where stromatolites, microfossils, and isotopic signals belong to the most dominant biosignatures (e.g. Allwood et al., 2006; Brasier et al., 2006; Wacey, 2009, 2012). The focus of this study here is to summarize and review the South African evidence of Paleoproterozoic life reported from the BGB, place them in a consistent stratigraphic framework, and discuss and evaluate the most recent findings.

2. Geology of the BGB

The Barberton Greenstone Belt of South Africa and Swaziland is located at the eastern margin of the Kaapvaal Craton and contains volcanic, shallow intrusive, and sedimentary rocks, ranging in age from <3.547 to >3.219 Ga (Byerly et al., 2019; Fig. 1). These age constraints are mainly derived from high-precision zircon U-Pb age dating of interbedded volcanic units and plutons surrounding the BGB, as well as detrital zircon geochronology. Rocks of the Barberton Supergroup (formerly named Swaziland Supergroup), are subdivided from base to top into three lithostratigraphic units: (1) the ~ 8 – 10 km thick, volcanic-dominated Onverwacht Group, which comprises the Komati, Hooggenoeg, Kromberg, and Mendon Formations (Viljoen and Viljoen, 1969; Anhaeusser, 1976; Lowe and Byerly, 2007; De Wit and Furnes, H., 2011); (2) the up to ~ 2 km thick Fig Tree Group, predominantly composed of interlayered volcanoclastic strata that mark the final stages of major volcanism and the transition to deposition of terrigenous clastic units (Heinrichs and Reimer, 1977; Lowe, 1999a; Hofmann, 2005; Byerly et al., 2019); and (3) the up to 3.5 km thick, coarse-grained siliciclastic to conglomeritic Moodies Group, mainly derived

113
114
115
116
117
118
119
120
121
122
123
124
125
126
127
128
129
130
131
132
133
134
135
136
137
138
139
140
141
142
143
144
145
146
147
148
149
150
151
152
153
154
155
156
157
158
159
160
161
162
163
164
165
166
167
168

70 from the erosion of underlying units and uplifted plutonic rocks (Eriksson, 1977; Heubeck and Lowe,
71 1994a, 1994b, 1999). The dominant large-scale orogeny of the BGB occurred contemporaneously with
72 deposition of the Moodies Group at 3.225–3.215 Ga (Lamb and Paris, 1988; Heubeck et al., 2013).
73 Although the BGB strata experienced several phases of major deformation during which they were folded,
74 faulted and altered, the rocks are generally well-preserved in locally very thick and laterally-traceable
75 sections (De Ronde and De Wit, 1994; Toulkeridis et al., 1998; Lowe and Byerly, 1999). A major fault
76 system, the Inyoka Fault, transects the BGB approximately medially and divides it into a northern and
77 southern facies, characterized by distinct differences in the preserved stratigraphy and depositional facies
78 of especially the Onverwacht and Fig Tree Groups (Fig. 2). Although approximately coeval, these deposits
79 represent previously geographically separated successions that are now in tectonic contact with another
80 (Byerly et al., 2019). The greenstone belt fill can be further subdivided into several tectonostratigraphic
81 blocks, each bordered by numerous, steeply dipping large and small faults (Lowe, 1999a; Lowe et al.,
82 2012). Most rocks in the central part of the BGB experienced alteration temperatures of >300°C (Xie et
83 al., 1997; Toulkeridis et al., 1998; Tice et al., 2004), however some primary mineralogy, textures, and
84 sedimentary structures have been preserved in many units due to the combination of early silicification and
85 the local partitioning of strain (Byerly et al., 2019).

86
87

88 **3. History of early life studies in the BGB**

89 The BGB has a long history of studies focusing on traces of early life and the reconstruction of its habitat,
90 metabolism, biogeochemical cycling, and mode of preservation (Table 1). Since the mid-1960s the
91 occurrence of lenticular, spheroidal, and filamentous microstructures, interpreted as possible cellular
92 microfossils, has been reported from carbonaceous cherts of the Onverwacht Group* (Barghoorn and
93 Schopf, 1966; Pflug, 1966, 1967; Schopf and Barghoorn, 1967; Pflug et al., 1969; Barghoorn, 1971). *[Note
94 that these samples were collected from the same outcrop, which was originally assigned to the Fig Tree
95 Group, but later revised and changed to the upper Onverwacht Group (Pflug, 1967; Schopf, 1975; Lowe
96 and Knauth, 1977).] In the following years simple spherical and filamentous microstructures have also
97 been described from other Onverwacht Group cherts of the Mendon and Kromberg Formation (Engel et al.,
98 1968; Nagy and Nagy, 1969; Brooks and Shaw, 1971; Brooks et al., 1973; Muir and Hall, 1974; Muir and
99 Grant, 1976; Knoll and Barghoorn, 1977), however the exact stratigraphic position was often not clearly
100 indicated, which made it challenging to put the individual findings in context to each other. In fact, the
101 insufficient knowledge of the BGB stratigraphy at that time and the often poorly studied depositional facies,
102 and paleoenvironmental context of the analyzed samples are central problems of most of these pioneering
103 studies. Due to their often simply morphology and wide size range the biogenicity of almost all of the early-

169
170
171
172
173
174
175
176
177
178
179
180
181
182
183
184
185
186
187
188
189
190
191
192
193
194
195
196
197
198
199
200
201
202
203
204
205
206
207
208
209
210
211
212
213
214
215
216
217
218
219
220
221
222
223
224

104 reported microfossils has been questioned in several reviews (Schopf, 1975; Schopf and Walter, 1983;
105 Altermann, 2001; Wacey, 2009), which suggested that except for the structures described by Muir and
106 Grant (1976) and Knoll and Barghoorn (1977) all other findings should be treated as nonfossil artefacts,
107 aggregates of amorphous carbonaceous matter or modern contaminants. More detailed sedimentological,
108 geochronological, and tectonostratigraphic investigations of the BGB deposits (Lowe and Knauth, 1977;
109 Kröner et al., 1991; Lowe and Byerly, 1999; Lowe et al., 2012), organic carbon isotope analysis (e.g. Oehler
110 et al., 1972), the identification of possible stromatolites (de Wit et al., 1982; Byerly et al., 1986; Byerly and
111 Palmer, 1991; Walsh, 2004), and new discoveries of mat-like laminations, lenticular, spheroidal, and
112 filamentous microfossil in cherts of the Hooggenoeg, Kromberg, and Mendon Formations (Walsh and
113 Lowe, 1985, 1999; Walsh, 1992; Westall et al., 2001; Glikson et al., 2008) supported previous findings
114 (e.g. Pflug, 1966; Knoll and Barghoorn, 1977) and stimulated further investigations. In the following,
115 carbonaceous laminations preserved in the shallow-water facies of the Buck Reef Chert (Kromberg
116 Formation) have been studied in great detail and were interpreted as the remains of photosynthetic microbial
117 mats (Tice and Lowe, 2004, 2006a, 2006b; Tice, 2009; Tice et al., 2011). Westall et al. (2006, 2011, 2015,
118 2018) identified microbial biofilms and possible fossil bacteria in the Josefsdal Chert (Kromberg
119 Formation) and suggested that these microbial communities were once thriving in a nearshore hydrothermal
120 setting. Tubular, titanite-mineralized microstructures in basaltic pillow lava rims of the Hooggenoeg and
121 Kromberg Formations were interpreted as being the result of microbial etching, and thus indicating the
122 presence of submarine thermophilic microbial communities during basalt formation (Furnes, 2004;
123 Banerjee et al., 2007; Furnes et al., 2007; Fliegel et al., 2010). However, the syngenicity and biogenicity of
124 these putative oldest trace fossils has been strongly questioned and is currently still under debate
125 (McLoughlin et al., 2012; Grosch and McLoughlin, 2014; Staudigel et al., 2015; Wacey et al., 2017;
126 Hickman-Lewis et al., 2019 for a short review). More recently, the biogenicity of lenticular microfossils
127 from the Kromberg Formation was further supported by *in situ* carbon isotope analysis (Oehler et al., 2017),
128 while new findings of cell-like objects from the Buck Reef Chert were interpreted as degraded colonies of
129 coccoidal bacteria (Kremer and Kaźmierczak, 2017). Moreover, Hickman-Lewis et al. (2018) reported
130 carbonaceous laminations, resembling microbial biofilms and mats from the Middle Marker at the base of
131 the Hooggenoeg Formation, making it to the most ancient claim for life in the BGB.
132 In the last decade also the sand- and siltstones of Moodies Group (uppermost unit of the BGB), were
133 carefully investigated for traces of early microbial life, which resulted in the discovery of large spheroidal
134 microfossils (Javaux et al., 2010), widespread shallow-marine tufted microbial mats once formed by
135 photosynthetic microorganisms (Noffke et al., 2006; Heubeck, 2009; Gamper et al., 2012; Homann et al.,
136 2015) and remnants of cavity-dwelling microbial communities (Homann et al., 2016). Terrestrial microbial
137 mats interbedded with fluvial sandstones and conglomerates, record a significant difference in their organic

225
226
227
228
229
230
231
232
233
234
235
236
237
238
239
240
241
242
243
244
245
246
247
248
249
250
251
252
253
254
255
256
257
258
259
260
261
262
263
264
265
266
267
268
269
270
271
272
273
274
275
276
277
278
279
280

138 carbon and nitrogen isotopes in comparison with the tidal marine mats and represent the oldest
139 macroscopically-visible trace of life on land (Homann et al., 2018). The presence of a Paleoproterozoic
140 terrestrial biosphere is further supported by the Moodies Group paleosols that carry signals of biogenic
141 sulfur fractionation (Nabhan et al., 2016a, 2016b). In the following, a selection of the most promising and
142 best documented claims for early life from the Onverwacht and Moodies Groups of the BGB will be
143 described and discussed in more detail.

144

145 **4. The 3.55–3.26 Onverwacht Group**

146 The Onverwacht Group consists of a up to 10 km thick succession of mostly of mafic and ultramafic
147 volcanic rocks with minor felsic volcanic flow units and tuffs (Lowe and Byerly, 1999). Subordinate
148 sedimentary units formed during episodic breaks in eruptive activity and have been widely silicified to
149 bedded cherts, which host a large number of the reported traces of early life in the BGB, including microbial
150 mats, microfossils, and possible stromatolites. Moreover, rare asteroid ejecta layers, composed of impact
151 spherules, fine ash and dust, locally occur as discrete beds and record distal impact events of large asteroids
152 with diameters ranging between 20–50 km (Fig. 2; Lowe and Byerly, 1986, 2018). The Onverwacht Group
153 comprises four different formations (Komati, Hooggenoeg, Kromberg, and Mendon), which each can be
154 further subdivided into informal members (e.g. H1 - H6). Within each member the cherts, which are capping
155 individual volcanic units are designated with a "c" (e.g. H4c; Lowe and Byerly, 1999; Byerly et al., 2019).
156 Overlying the basal Komati Formation, the 3.472 - 3.416 Ga Hooggenoeg Formation consists of thick
157 sequence of tholeiitic basalts, minor komatiites, and thin chert units and can reach a thickness of up to 3900
158 m on the western limb of the Onverwacht Anticline (Viljoen and Viljoen, 1969b, Lowe and Byerly, 1999).
159 The 3.416 – 3.334 Ga Kromberg Formation on the west limb of the Onverwacht Anticline comprises an up
160 to 1800-m-thick succession of black and banded chert (Buck Reef Chert, K1), mafic lapilli tuff and
161 lapillistone (K2), and tholeiitic basalt (K3), while on the eastern limb of the anticline massive pillow basalt
162 is more abundant. The top of the formation is marked by a regionally traceable chert unit, the Footbridge
163 Chert (K3c; Viljoen and Viljoen, 1969, Lowe and Byerly, 1999). Conformably overlying the Kromberg
164 Formation, the 3.334 – 3.258 Ga Mendon Formation has a thickness of >600m and records an alternation of
165 volcanic cycles, each characterized by a komatiitic flow unit capped by a chert layer (Byerly, 1999).

166

167 **4.1 Microbial mats**

168 The first systematic stratigraphic and petrographic analysis of all carbonaceous cherts in the Hooggenoeg,
169 Kromberg, and Mendon Formation of the Onverwacht Group was made by Walsh (1992) and Walsh and
170 Lowe (1999), who distinguished three main types: black-and-white banded, massive black, and black
171 laminated chert. The carbonaceous matter in these cherts occurs mostly in the form of: fine laminations (1

281
282
283
284
285
286
287
288
289
290
291
292
293
294
295
296
297
298
299
300
301
302
303
304
305
306
307
308
309
310
311
312
313
314
315
316
317
318
319
320
321
322
323
324
325
326
327
328
329
330
331
332
333
334
335
336

172 – 20 μm thick), carbonaceous wisps (10–50 μm thick, 50–1000 μm long) that are likely eroded fragments
173 of the fine laminations, subrounded composite grains (100–1000 μm), and irregular-shaped simple grains
174 (5–750 μm), and. Based on bulk $\delta^{13}\text{C}_{\text{org}}$ values ranging between -40.8‰ and -16.9‰ , with a mean of
175 -29.8‰ ($n = 50$), Walsh and Lowe (1999) concluded that all the carbonaceous matter in the cherts is
176 probably of biological origin, which was further supported by a detailed study of van Zuilen et al. (2007),
177 combining Raman spectroscopy and SIMS (secondary ion mass spectrometry) analysis.
178 In detail, the fine carbonaceous laminations that form layers of 0.5–2 cm thickness and occur predominantly
179 in black-and-white banded cherts the Hooggenoeg (H2, H4c, H5c), Kromberg (K1, K3c), and Mendon
180 Formation (M1c, M2c), were interpreted as remains of microbial mats (Walsh, 1992; Walsh and Lowe,
181 1999; Trower and Lowe, 2016). The alternation of carbonaceous black bands with thin layers of pure
182 (white) quartz in these cherts is likely comparable with alternating organic-rich and organic-poor sediments
183 in modern microbial mats. The mats presumably formed in periods of volcanic quiescence but likely under
184 the presence of hydrothermal activity. They are often interbedded with layers of composite carbonaceous
185 grains, which Walsh (1992) compared to globular bacterial colonies or organic aggregates, however, the
186 biogenicity of these grains still needs to be further established (Trower and Lowe, 2016). In the following,
187 reported microbial mats and biofilms from the Middle Marker, the Buck Reef Chert, and Josefsdal Chert
188 will be described in more detail.

189 190 **4.1.1 Middle Marker**

191 The 3.472 Ga Middle Marker (H1) at the base of the Hooggenoeg Formation represents the oldest, relatively
192 unmetamorphosed sedimentary unit of the BGB (Lanier and Lowe, 1982; Armstrong et al., 1990). It has a
193 thickness of 3 to 6 m and is composed of silicified komatiitic ash and fine layers of relatively pure
194 carbonaceous cherts that contain composite grains and carbonaceous wisps of proposed biogenic origin
195 (Lanier and Lowe, 1982; Walsh, 1992; Lowe, 1999; Walsh and Lowe, 1999). Deposition occurred likely
196 on a flat, tide- or wave influenced shelf in water depths of several 10s to 100 m (Byerly et al., 2019).
197 Fine, crinkly laminations, interbedded with the volcanoclastic sand- and siltstones of this unit, have been
198 interpreted as fossil microbial mats by Hickman-Lewis et al. (2018), mainly based on their carbonaceous
199 composition, micro-tufted morphology, sediment trapping and cohesive behavior, and the occurrence of
200 wisp-like structures, interpreted as erosional mat (Fig. 3A and B). The carbonaceous laminations occur in
201 packets of 200 μm to 2.5 mm thickness, contain detrital quartz and volcanic grains, and generally have a
202 low surficial relief, which is described by the authors as micro-tufted (Fig. 3A and B). These crinkly, micro-
203 tufted structures (<100 μm in height) of proposed primary biogenic origin can be distinguished from pseudo-
204 tufted structures (up to 0.8 mm in height) that formed secondary as a result of plastic deformation triggered
205 by the settling of dense particles (Fig. 3C and D; Hickman-Lewis et al., 2018). The micro-tufted structures

337
338
339
340
341
342
343
344
345
346
347
348
349
350
351
352
353
354
355
356
357
358
359
360
361
362
363
364
365
366
367
368
369
370
371
372
373
374
375
376
377
378
379
380
381
382
383
384
385
386
387
388
389
390
391
392

206 were further used by Hickman-Lewis et al., (2018) to tenta
207 were formed by anoxygenic phototrophs. However, it is hard to constrain the microbial metabolism relying
208 on mat morphology alone, especially if it is only of minor topographic relief and secondary deformation
209 structures are present. More valuable insights into the metabolism(s) of the Middle Marker mats could be
210 gained from the analysis of organic carbon isotopes, which would also help to further strengthen their
211 biogenicity.

212

213 **4.1.2 Buck Reef Chert**

214 The 3.416 Ga Buck Reef Chert (K1) is a 250–400-m-thick unit of carbonaceous and ferruginous cherts at
215 the base of the Kromberg Formation, exposed continuously along nearly 50 km of strike in the west limb
216 of the Onverwacht Anticline (Kröner et al., 1991; Lowe and Worrell, 1999). A correlative section in the
217 east limb of the Onverwacht Anticline comprises three 10–25-m-thick chert units (Kc1, Kc2, Kc3), that are
218 interbedded with basalt flows (Walsh, 1992; Lowe and Byerly, 1999). The cherts are thought to be of
219 primary origin and likely precipitated from normal marine water, which was saturated with respect to
220 amorphous silica during the Archean (Lowe, 1999b; Knauth and Lowe, 2003; Tice and Lowe, 2006a) rather
221 than from hydrothermal fluids (de Wit et al., 1982; Westall et al., 2001). Sediments of the Buck Reef Chert
222 were deposited on subsiding open-marine volcanic platform and can be subdivided in three main
223 depositional facies (basal evaporitic, middle platform, and deep basin), which reflect deposition under
224 successively deeper-water conditions (Tice and Lowe, 2004). The silicified evaporites from the evaporitic
225 facies, were originally interpreted as remnants of nahcolite (Lowe and Worrell, 1999) but may represent
226 pseudomorphs after aragonite (Otálora et al., 2018). Fine anastomosing carbonaceous laminations (Fig. 4A-
227 F) and in places ripped up, plastically deformed rolled-up fragments (Fig. 5 A and B), occurring within
228 black bands in black-and-white banded cherts of the platform facies, were interpreted as remnants of
229 cohesive microbial mats (Walsh and Lowe, 1999; Tice and Lowe, 2004, 2006a, 2006b; Tice, 2009; Tice et
230 al., 2011). The mats were once thriving in shallow-water, photic zone paleoenvironments below fair-
231 weather wave base and show three distinct mat morphotypes: (1) alpha-type, fine carbonaceous laminations
232 that incorporate and loosely drape detrital grains underlying detrital grains and form silica-filled lenses (Fig.
233 4A and B); (2) beta-type, fine meshworks of filament-like strands (<5µm in diameter), which drape
234 underlying detrital grains (Fig. 4C and D); and (3) gamma-type, evenly spaced flat laminations that tightly
235 drape underlying sediments (Fig. 4E and F; Tice, 2009). The formation of different mat morphotypes is
236 thought to be primarily controlled by local variations in ambient light intensity and/or current energy.
237 Consequently, the first two morphotypes (alpha and beta) probably formed in shallower water, which is
238 also supported by their more complex morphology and association with coarser-grained sediments (Tice
239 2009). Bulk organic carbon isotope measurements of the carbonaceous laminations, with $\delta^{13}\text{C}_{\text{org}}$ values

393
394
395
396
397
398
399
400
401
402
403
404
405
406
407
408
409
410
411
412
413
414
415
416
417
418
419
420
421
422
423
424
425
426
427
428
429
430
431
432
433
434
435
436
437
438
439
440
441
442
443
444
445
446
447
448

240 ranging between -36.9% and -20.1% , and a mean of -29.9% ($n = 19$, Tice and Lowe 2006b), serve as
241 additional evidence for a biogenic origin of the mats, which were formed by photosynthetic microbes that
242 most likely applied hydrogen-based carbon fixation (Tice and Lowe, 2004a, 2006a). Raman
243 microspectroscopic analysis further revealed that the carbonaceous matter preserved in the Buck Reef Chert
244 has experienced sub- to lower-greenschist facies temperatures, consistent with regional peak metamorphic
245 temperatures, and thus confirming its syngenetic origin (Tice et al., 2004; van Zuilen et al., 2007). Overall,
246 the microbial mats preserved in the Buck Reef Chert represent one of the best documented evidence for
247 ancient life in the Onverwacht Group. Future work could focus more on micro-scale investigations, increase
248 the spatial resolution of organic carbon isotope measurements, and try to acquire also nitrogen isotope
249 values in order to learn more about the biogeochemical cycling of these elements by the mat-forming
250 microbial communities.

251
252

253 **4.1.3 Josefsdal Chert**

254 The Josefsdal Chert comprises a 6–30-m-thick succession of silicified volcanoclastic rocks, located in a
255 fault-bounded sliver, and is considered to be the lateral equivalent of the 3.334 Ga Footbridge Chert (K3c;
256 (Kröner et al., 1996; Lowe and Byerly, 1999) at the top of the Kromberg Formation (Hofmann and Bolhar,
257 2007; Westall et al., 2015). Sedimentary structures, such as ripple marks, planar- and cross-lamination
258 indicate that deposition likely occurred in tidal, nearshore environments under the influence of
259 hydrothermal activity, which is supported by REE patterns with positive Eu and Y anomalies and was likely
260 driven by the circulation of silica-saturated seawater through cooling basaltic lavas that occur
261 stratigraphically below the Josefsdal Chert (Hofmann and Harris, 2008; Westall et al., 2011, 2015, 2018).
262 Cracks, only a few μm in width, occurring in structures interpreted as fossil biofilms from these deposits,
263 were further used to infer periods of subaerial exposure, desiccation, and evaporation (Westall et al., 2001;
264 2006). Such cracks are, however, less suitable to reconstruct the depositional context, as they are only
265 visible with the SEM (scanning electron microscope) and not in the outcrops. Altermann (2001) suggested
266 that these cracks and the pseudomorphic evaporite minerals, as well as some putative rod-shaped
267 microfossils (2–3.8 mm long and interpreted as remnants of sulphate-reducing bacteria) described by
268 Westall et al. (2001, 2006) from these cherts, might represent sample preparation artefacts introduced
269 during HF etching (Wacey, 2009). Moreover, the fact that the anions of the putative, often idiomorphic,
270 evaporite crystals have been replaced by fluorine (Westall et al., 2006) further indicates that they could
271 represent artefacts, especially as it has been shown that mineral artefacts such as fluorides and fluosilicates
272 commonly form during HF etching (Karkhanis, 1977) and might mimic evaporitic minerals. A more
273 promising candidate for life in these deposits are therefore the structures that are visible in petrographic

449
450
451
452
453
454
455
456
457
458
459
460
461
462
463
464
465
466
467
468
469
470
471
472
473
474
475
476
477
478
479
480
481
482
483
484
485
486
487
488
489
490
491
492
493
494
495
496
497
498
499
500
501
502
503
504

274 thin section and resemble silicified biofilms and microbial mats (Fig 6 A-C). The microbial mat-like
275 structures occur in banded black and white cherts as layered packets, 100–1000 μm thick, that are composed
276 of $\sim 10\mu\text{m}$ thin, wavy carbonaceous biofilms with incorporated fine-grained detrital volcanic clasts and
277 quartz grains (Westall et al., 2006; 2011; 2015). Torn and plastically deformed fragments of these biofilms
278 occur partially peeled of below and above distinct mat horizons, which is interpreted as evidence for
279 contemporaneous (lateral?) injection of hydrothermal fluids (Fig. 6D, Westall et al., 2015). A single biofilm
280 (1–4 μm thick) exposed on fresh fractured bedding surface has been extensively studied by Westall et al.
281 (2001, 2006, 2011; sample 96SA05) and SEM observations revealed the presence of multiple layers of
282 parallel filament-like structures with constant diameter of 0.25 μm , which are embedded in a granular to
283 smooth film interpreted as extracellular polymeric substance. Carbonaceous clots, 50–500 μm in diameter
284 and interpreted as degraded remnants of chemosynthetic biomass, represent another proposed biosignature
285 from Josefsdal Chert (Westall et al., 2015), however their biogenicity still needs to be further established.
286 Two bulk organic carbon isotope measurements from the Josefsdal Chert show $\delta^{13}\text{C}_{\text{org}}$ values of -22.7‰
287 (bulk sample, Westall, et al 2001) and -26.8‰ (carbon-rich black layer, Westall et al., 2006). While *in situ*
288 measurements of the carbonaceous biofilms yield $\delta^{13}\text{C}_{\text{org}}$ values of -45‰ to -13‰ and a single $\delta^{34}\text{S}$ value
289 of -24‰ (Westall et al., 2015). These values support a biogenic origin of the biofilms/mats and were further
290 used to conclude that the latter were formed by anoxygenic photosynthesizers and sulphur reducing bacteria
291 (Westall et al. 2011, 2015). Future *in situ* isotope studies on the organic remains in these samples should
292 increase the amount of data points and aim to better document the analytical areas (see e.g. Williford et al.
293 2013, 2016) in order to spatially resolve the large range of $\delta^{13}\text{C}_{\text{org}}$ values, and to distinguish it from the
294 background signal of the carbonaceous cherts, which might differ significantly, as documented by Oehler
295 et al. (2017) for samples of the Buck Reef Chert that show $\delta^{13}\text{C}_{\text{org}}$ values ranging between -47.1‰ and
296 -24.0‰ .

297 298 **4.2 Microfossils**

299 The positive identification of Archean microfossils is due to their often very simple morphology extremely
300 challenging, several well-established criteria exist (see Schopf, 2004; Brasier et al., 2006; Wacey, 2009),
301 while *in situ* carbon isotope analysis of individual microfossil candidates has become another required
302 method for the evaluation of their biogenicity in recent years (e.g. House et al., 2013; Lepot et al., 2013;
303 Williford et al., 2013, 2016). Putative microfossils in the carbonaceous cherts of the Onverwacht Group are
304 extremely rare. The first systematic analysis of Walsh (1992) and Walsh and Lowe (1999) revealed that
305 only 9 of more than 400 analyzed samples contained possible microfossils of filamentous, lenticular, and
306 spheroidal shapes.

307

505
506
507
508
509
510
511
512
513
514
515
516
517
518
519
520
521
522
523
524
525
526
527
528
529
530
531
532
533
534
535
536
537
538
539
540
541
542
543
544
545
546
547
548
549
550
551
552
553
554
555
556
557
558
559
560

308 **4.2.1 Filamentous structures**

309 Filamentous microstructures of carbonaceous composition were identified in a single 2 cm thick black-and-
310 white banded chert layer in the upper Hooggenoeg Formation (Walsh and Lowe, 1985; Walsh 1992). These
311 tread-like or cylindrical, unbranched filaments are solid, 0.2 – 2.5 μm in diameter, up to 200 μm long and
312 occur associated with carbonaceous laminations interpreted as microbial mats. Although originally
313 classified as possible microfossils Walsh (2000) noted that they may have formed abiotically and could
314 thus represent simple mineral filaments (Wacey, 2009).
315 More convincingly biological filaments occur associated with fossil mats in several localities of the Buck
316 Reef Chert (K1 and K1c2; Byerly et al., 2019). The hollow cylindrical filaments, 1.2 – 1.4 μm in diameter
317 and 10 – 150 μm in length, are composed of carbonaceous matter and fine pyrite (Fig. 7A-C). They mostly
318 occur oriented subparallel to bedding or sometimes as interwoven, tangled clumps (Walsh and Lowe, 1985;
319 Walsh 1992). These hollow, sheath-like filaments are similar in size and shape to modern filamentous
320 bacteria and are of possible organic origin (Walsh 1992, Altermann, 2001), however, high-resolution
321 petrographic and detailed *in situ* carbon isotope analysis would be desirable to further support this
322 interpretation.

323
324

325 **4.2.2 Lenticular structures**

326 Lenticular structures (previously named “spindle-shaped” structures) represent a group of enigmatic
327 microfossils that are also well-known from the Pilbara Craton of Western Australia where their biogenicity
328 is well established (e.g. Sugitani et al., 2007, 2010, 2013, Oehler et al., 2009, 2017; House et al., 2013;
329 Kozawa et al., 2018). There, the lenticular objects occur individually or in groups or chains of several
330 individuals. Lense- or, disk-shaped microstructures, 30–60 μm in long axis, with hollow centers and
331 carbonaceous walls have been first documented in the BGB by Pflug (1966, 1967) and Pflug et al., (1969)
332 from cherts of the Fig Tree Group that were later assigned to the upper Onverwacht Group (Mendon
333 Formation, previously named Swartkoppie Formation, (Schopf, 1975; Lowe and Knauth, 1977)). The
334 structures gently taper towards the ends of their long axes, occur isolated or sometimes in groups of two or
335 more specimens (Fig. 8A-D), which are connected at their poles, and were interpreted as the remains of
336 thread-like bacterial colonies (Pflug, 1966, 1967). Walsh (1992) interpreted very similar lenticular
337 structures, 13–135 μm long and 4.5–61 μm wide, from detrital layers above the basal evaporitic facies of
338 the Buck Reef Chert (K1) as possible sheaths of colonies of bacterial cells or carbonaceous coatings around
339 former gypsum crystals (Fig. 8E-H). A biological origin of the structures is supported by *in situ* $\delta^{13}\text{C}_{\text{org}}$
340 analysis that revealed values ranging between -39.3‰ to - 35.5 ‰, consistent with autotrophic carbon
341 fixation (n = 8; Oehler et al., 2017). Based on their robust morphology, shallow water habitat and $\delta^{13}\text{C}_{\text{org}}$

561
562
563
564
565
566
567
568
569
570
571
572
573
574
575
576
577
578
579
580
581
582
583
584
585
586
587
588
589
590
591
592
593
594
595
596
597
598
599
600
601
602
603
604
605
606
607
608
609
610
611
612
613
614
615
616

342 values Oehler et al. (2017) proposed that the lenticular forms might represent microbes with a planktonic
343 stage in their life cycle, making it to a very promising claim for microbial life in the BGB.

344

345 **4.2.3 Spheroidal structures**

346 Spheroidal microstructures of carbonaceous composition belong to a very common group of putative
347 microfossils in the Onverwacht Group but the evaluation of their biogenicity is due to their simple
348 morphology often very challenging.

349 Glikson et al. (2008) identified clusters of spheroidal, cell-like objects (2–10 μm in diameter) with granular
350 walls from cherts of the Hooggenoeg Formation (H3c and H5c), which display features of possible cell
351 wall degradation (Fig. 9A and B). The spheroids are comparable with the modern hyperthermophilic
352 *Methanocaldococcus jannaschii* and were thus interpreted as remnants of chemosynthetic microbes once
353 thriving in a seafloor hydrothermal system. This is a promising sign for life, but follow-up studies should
354 also document the sedimentological context, perform analysis on more than two samples, and include *in*
355 *situ* isotope measurements (Wacey et al., 2009). Large granular-walled spheroids and ellipsoids (10–84 μm
356 in length; Fig. 9C and D) and clusters of thin-walled spheroids (4.5–12.8 μm in diameter; Fig. 9E and F)
357 from the Buck Reef Chert were interpreted as probable microfossils of coccoidal bacteria or spores (Walsh,
358 1992). However, these simple spheres may be produced abiotically in various ways and were therefore
359 reinterpreted as abiotic self-organized structures, such as spherulitic chert (Brasier et al., 2006). Kremer
360 and Kazmierczak (2017) reported spheroidal microstructures, 3–12 μm in diameter, from the Buck Reef
361 Chert (K1c2) and tentatively conclude that they may represent the variably degraded remains of coccoidal
362 cyanobacteria (Fig. 9G and H). Although the cell-like objects occur in groups or clusters, preserved in black
363 cherts with bulk $\delta^{13}\text{C}_{\text{org}}$ values of -26.5‰ and -24.3‰ ($n = 2$), their outer walls often have a more angular
364 than rounded appearance, which resemble crystal terminations, thus making a biological origin less
365 favorable (Hickman-Lewis, 2019). Alternatively, these objects might represent carbonaceous linings on
366 replaced minerals or crystal rims (Brasier et al., 2006). Moreover, beyond morphological similarity, the
367 positive identification of cyanobacteria and oxygenic photosynthesis hundreds of millions of years before
368 most other evidence, requires independent geochemical evidence for the local presence of free oxygen,
369 which is currently not available. Future studies should include nanoscale analysis of the putative cell walls
370 and *in situ* isotope measurements.

371 Another occurrence of possible organic microspheres, 1– 4 μm in diameter, has been described by Knoll
372 and Barghoorn (1977) from the Msauli Chert (M1c; Mendon Formation, previously named Swartkoppie
373 Formation (Lowe, 1999c)), which was deposited in shallow-water nearshore environments (Fig. 9I). These
374 carbonaceous spheres occur as isolated or paired objects, are often flatten, wrinkled or folded, show a
375 narrow unimodal size frequency distribution ($n = 200$), evidence of possible cell division, and were

617
618
619
620
621
622
623
624
625
626
627
628
629
630
631
632
633
634
635
636
637
638
639
640
641
642
643
644
645
646
647
648
649
650
651
652
653
654
655
656
657
658
659
660
661
662
663
664
665
666
667
668
669
670
671
672

376 interpreted as the remains of primitive prokaryotes (Knoll and Barghoorn, 1977). However, without any
377 geochemical analysis also these structures cannot be unambiguously identified as biological (Wacey, 2009).

378

379

380 **4.3 Stromatolites**

381 Compared to its Australian counterpart the currently known stromatolite occurrences in the BGB are very
382 rare. Byerly et al. (1986) reported putative pseudocolumnar stromatolites that crop out for more than 10 km
383 along strike in grey to black cherts assigned to member M2c of the ~3.23 Ga Mendon Formation (Walsh,
384 2004; Lowe and Byerly, 2015), which is interbedded with komatiitic lava flow deposits. [Note that these
385 outcrops were initially assigned to the Fig Tree Group (Byerly et al., 1986), but are now thought to belong
386 to the Mendon Formation in the upper Onverwacht Group (Lowe, 1994)]. The possible stromatolites occur
387 in layers of <1 to 20 cm thickness and display variable morphologies, ranging between low-relief,
388 asymmetrical, sometimes laterally-linked domes (1–3 cm wide and 0.5–3 cm high), rare pseudocolumns
389 with bridging laminae (up to 10 cm height), and crinkly stratiform laminations (50–100 μm thick; Fig. 10A
390 and B). Individual laminae are composed of minor amounts of primary carbonaceous matter and variable
391 amounts of secondary, fine-grained, often idiomorphic tourmaline minerals (sometimes up to 50%), which
392 may have been derived through the hydrothermal remobilization of previously formed, boron-rich
393 evaporites (Fig. 10C; Byerly and Palmer, 1991). Alternatively, the tourmaline mineralization could have
394 been caused by heating and partial ocean evaporation related to a large asteroid impact recorded by spherule
395 beds S5 and S8, which occur associated with some of the stromatolites (Lowe and Byerly, 2015).
396 Conglomerates composed of laminated silica chips occur in the throughs between stromatolite domes and
397 have been interpreted as fragments of eroded stromatolites or sinter crusts, likely deposited in the aftermath
398 of a large impact (Fig. 10D). Similar stromatolite-crust chip conglomerates have also been reported from
399 the Fig Tree Group (Sheba Formation) where they are overlain by spherule bed S5 (Lowe and Byerly, 2015,
400 2018). The stromatolitic structures were possibly formed by hyperthermophilic microbial communities in
401 shallow-water depositional environments during periods of relative volcanic quiescence and likely
402 experienced the profound effect of distant asteroid impacts (Byerly et al., 1986; Lowe and Byerly, 2018).
403 The widespread occurrence, morphological variability, and similarity to other fossil and modern
404 stromatolites suggest a biogenic origin of these structures (Awramik, 1992). However, organic carbon
405 isotope measurements, three-dimensional morphological investigations, a better documentation of the
406 different morphotypes (Allwood et al., 2006), combined with high-resolution petrographic analysis, and a
407 clear distinction from possibly abiogenic hot-spring silica crust precipitates (Lowe, 1994) would be
408 desirable to further support this interpretation.

409

673
674
675 410
676 411
677
678 412
679 413
680 414
681 415
682 416
683 417
684 418
685 419
686 420
687 421
688 422
689 423
690 424
691 425
692 426
693 427
694 428
695 429
696 430
697 431
698 432
699 433
700 434
701 435
702 436
703 437
704 438
705 439
706 440
707 441
708 442
709 443
710
711
712
713
714
715
716
717
718
719
720
721
722
723
724
725
726
727
728

5. The ~3.22 Ga Moodies Group

The ca. 3.22 Ga Moodies Group is the uppermost stratigraphic unit of the BGB and represents the world's oldest well-preserved alluvial to shallow-marine tidal deposit. It consists of a up to 3.5 km thick succession of quartz-rich sandstones with subordinate conglomerates, mudstones, siltstones, thin volcanic tuff beds, minor banded iron formations and a basaltic lava, deposited in marine (deltaic, inter-, and subtidal) and terrestrial (alluvial, fluvial, possibly aeolian) paleoenvironments (Hall, 1918; Visser, 1956; Anhaeusser, 1976; Eriksson, 1977, 1979, Heubeck and Lowe, 1994a, 1999; Simpson et al., 2012; Homann et al., 2015, 2018; Heubeck et al., 2016). The age of the Moodies Group is tightly constrained by Uranium–lead dating of single-zircons from several dacitic tuffs and rare felsic dykes, which indicate that deposition began about 3.223 ± 1 Ga and had ended by about 3.219 ± 9 Ga (De Ronde and Kamo, 2000; Heubeck et al., 2013). Moodies strata north of the Inyoka Fault are preserved in several, commonly northward-overturned synclines that are tectonically separated by major faults (Fig. 2). These deposits not only contain a large variety of well- preserved sedimentary structures, they also offer a high-resolution archive of Paleoproterozoic surface and sedimentation processes, as well as a unique window into a widespread, diverse and well adapted microbial ecosystem. Reported biosignatures from the Moodies Group include intertidal and fluvial microbial mats, silicified remnants of cavity-dwelling microorganisms (coelobionts), and large organic-walled microfossils (acritarchs), as detailed below.

5.1 Microbial mats

Fossil microbial mats in the Moodies Group have been identified so far in intertidal deposits of the Saddleback Syncline and in alluvial-fluvial deposits of the Dycedale Syncline (Fig. 11A-C). In the Saddleback Syncline the mats are preserved as carbonaceous, crinkly laminations (0.5–1 mm thick), interbedded with medium- to coarse-grained sandstones, and associated with desiccation cracks (Fig. 12A) They represent the oldest known examples of siliciclastic tidal mats in the geological record (Noffke et al., 2006; Heubeck, 2009; Gamper et al., 2012; Homann et al., 2015). These mats draped and stabilized horizontally laminated and rippled sandstones, and show an enrichment in fine-grained quartz and feldspar, as well as heavy mineral grains (zircon and rutile or anatase), likely caused by microbial baffling and trapping, which is a commonly observed in epibenthic microbial mats (Gerdes et al., 2000). Microbial-mat-associated structures such as eroded mat fragments (mat chips), macroscopic tufts, shrinkage cracks, silicified gas domes and lenses, and subvertical fluid-escape structures are indicative for a former cohesive consistency and very common features in these deposits supporting the biogenic origin of the mats (Fig. 12B-D; Heubeck, 2009; Homann et al., 2015, 2016, 2018), while microbial wrinkle structures previously reported by Noffke et al. (2006) have not been observed in any of the follow-up studies. A detailed study

729
730
731
732
733
734
735
736
737
738
739
740
741
742
743
744
745
746
747
748
749
750
751
752
753
754
755
756
757
758
759
760
761
762
763
764
765
766
767
768
769
770
771
772
773
774
775
776
777
778
779
780
781
782
783
784

444 of the sedimentological and paleoenvironmental context of these fossil mats revealed that they are laterally
445 traceable for ~15 km in a ~1000 m-thick succession in the lower part of the Saddleback Syncline and show
446 distinct morphological adaptations to different hydrodynamic settings: (1) planar-type in coastal floodplain,
447 (2) wavy-type in intertidal, and (3) tufted-type in upper inter- to supratidal facies (Homann et al., 2015).
448 Such facies dependent changes in the prevalent mat morphotypes are to be expected in a dynamic, tidally-
449 influenced coastal environment and serve as an additional biogenicity indicator (Allwood et al., 2006;
450 Brasier et al., 2006). Moreover, the widespread occurrence of these fossil mats is consistent with a primary,
451 microbially mediated, cohesive erosion-resistant relief on the paleosurface that was locally deformed by
452 migrating gases and fluids, and in places eroded and incorporated in mat-chip conglomerates.
453 Based on the restriction of the mats to shallow-water, photic zone environments and their apparent absence
454 in subtidal settings, it is very likely that they were formed by phototrophic microbial communities (Noffke
455 et al., 2006; Heubeck, 2009, Homann et al., 2015). In fact, the Moodies microbial mats show some striking
456 morphological similarities to modern cyanobacterial mats e.g. from Bahar Alouane, Tunisia (Fig. 12A-D;
457 Gerdes et al., 2000; Gerdes, 2007), Shark Bay, Australia (Jahnert and Collins, 2013), 2013), Texas Gulf
458 Coast, USA (Bose and Chafetz, 2009), and the Red Sea of Saudi Arabia (Taj et al., 2014). Especially the
459 occurrence of mats with macroscopic, 0.3-to-1 cm-high tufts that closely resemble tufted mats build by
460 filamentous cyanobacteria (Fig. 12C), led to the conclusion that the tufted mats of the Moodies Group were
461 perhaps build by ancestral cyanobacteria (Homann et al., 2015). Even tough, no geochemical data
462 supporting the local presence of free oxygen (and thus oxygenic photosynthesis) at 3.22 Ga have been found
463 so far in the Moodies Group, fossil evidence indicative for ancient gas production, accumulation, and
464 migration is plentiful in the near vicinity of the mats. Now chert-filled cavities in the interior of some tufts
465 likely represent silicified gas bubbles that were trapped within the mat fabric, which is a common feature
466 in cyanobacterial mats that produce oxygen-rich bubbles with strikingly similar morphologies (Fig. 12C;
467 Bosak et al., 2010; Homann et al., 2015). Other types of silicified cavities include domes and bedding
468 parallel lenses beneath the fossil mats that either formed through accumulation of gases produced by
469 metabolic activity, due to the decay of organic matter, or alternatively by tidal-driven hydraulic pumping
470 of the ambient air trapped in pore space (Figs. 12D and 14; Homann et al., 2016). Some of these cavities
471 where also inhabited by microbial communities (see below in 5.2).
472 Besides the main mat occurrence in the tidal marine deposits of the Saddleback Syncline, fossil microbial
473 mats also have been identified in the Dycedale Syncline (Homann et al., 2018), where a large variety of
474 sedimentary structures indicates that this succession records a transition from alluvial-fluvial (terrestrial) to
475 tide-influenced marine sedimentation (Heubeck and Lowe, 1994; Eriksson et al., 2006; Heubeck et al.,
476 2016). These terrestrial mats occur confined to fluvial deposits at the base of a transgressive sequence that
477 gradually deepens upward through deltaic, and medium-energy tidal, into subtidal siliciclastic deposits.

785
786
787
788
789
790
791
792
793
794
795
796
797
798
799
800
801
802
803
804
805
806
807
808
809
810
811
812
813
814
815
816
817
818
819
820
821
822
823
824
825
826
827
828
829
830
831
832
833
834
835
836
837
838
839
840

478 They are interbedded with gravely sandstones, drape conglomerate beds, are plastically deformed by 10-
479 to 50-cm-high fluid-escape structures, and commonly experienced periods of subaerial exposure and
480 desiccation evidenced by associated desiccation cracks (Fig. 13A and B). The terrestrial microbial mats of
481 the Dycedale Syncline currently represent the oldest direct fossil trace for life on land (Homann et al.,
482 2018). Overgrowth rims in pyrites from Moodies Group paleosols show signs of biogenic sulfur
483 fractionation ($\delta^{34}\text{S}_{\text{VCDT}}$ values between -20% and -24.5%) and provide additional geochemical evidence
484 for the presence of a Paleoarchean terrestrial biosphere (Nabhan et al., 2016a, b). Compared to the marine
485 mats the carbonaceous laminae of terrestrial mats are similarly well preserved, but with up to 4 mm of
486 preserved thickness often thicker than their marine counterparts (Fig. 11A and B; Fig. 13C). They are
487 composed of a dense meshwork of interwoven filament-like microstructures that envelop fine-grained
488 detrital particles whose long axes are preferentially aligned parallel to bedding (Fig. 13D and E; Homann
489 et al., 2018). Individual carbonaceous filamentous structures are 1–3 μm in diameter and resemble modern
490 biofilm-forming, filamentous microorganisms. In places, a notable enrichment of tourmaline minerals can
491 be observed in the mat fabric, which has also been reported from the stromatolitic laminae of the Mendon
492 Formation (Byerly et al., 1986; Byerly and Palmer, 1991) and might be driven by evaporitic processes, but
493 certainly demands further investigations. Raman spectroscopic analyses confirmed that both the terrestrial
494 and marine mats are composed of organic carbon that has experienced similar peak temperatures of $\sim 365^\circ\text{C}$,
495 consistent with the metamorphic grade of the Moodies Group (Xie et al., 1997; Tice et al., 2004) and thus
496 demonstrating their synsedimentary origin and biogenicity (Homann et al., 2018). A detailed study of
497 Homann et al. (2018) documented a significant difference in the biogeochemical cycling of carbon and
498 nitrogen in terrestrial and marine mats. The preserved organic matter in the terrestrial mats shows $\delta^{13}\text{C}_{\text{org}}$
499 values ranging between -23.6% and -17.9% (mean = -21.2% ; $n = 36$) and $\delta^{15}\text{N}$ values between $+1.9\%$
500 and $+5.6\%$ (mean = $+4.3\%$; $n = 10$), in contrast to marine mats that show $\delta^{13}\text{C}_{\text{org}}$ values ranging between
501 -33.9% and -21.3% (mean = -27.4% ; $n = 30$) and $\delta^{15}\text{N}$ values between -0.7% and $+3.1\%$ (mean =
502 $+1.8\%$; $n = 10$). This $\delta^{13}\text{C}_{\text{org}}$ composition of the terrestrial mats is consistent with autotrophic carbon
503 fixation through the Calvin–Benson cycle, while $\delta^{13}\text{C}_{\text{org}}$ values of the marine mats are best explained by
504 carbon fixation via the Wood–Ljungdahl pathway, which includes acetogenic bacteria, methanogens and
505 sulfate reducers. The observed trend in the Moodies Group microbial mats with $\delta^{15}\text{N}$ values from as low as
506 -1% (marine) to up to $+5\%$ (terrestrial) likely reflects increasing fixed-nitrogen (i.e., nitrate, nitrite or
507 ammonium) and conversion to $\text{N}_2\text{O}/\text{N}_2$ in the terrestrial habitats, which further suggests that they possessed
508 a fundamentally different respiratory community at depth in the mat, one that must have been sufficiently
509 oxygenated for aerobic Nitrogen cycling (Ader et al., 2016; Stüeken et al., 2016). Alternatively, the
510 contrasting nitrogen isotope compositions between terrestrial and marine settings could be related to a

841
842
843
844
845
846
847
848
849
850
851
852
853
854
855
856
857
858
859
860
861
862
863
864
865
866
867
868
869
870
871
872
873
874
875
876
877
878
879
880
881
882
883
884
885
886
887
888
889
890
891
892
893
894
895
896

511 constant flux of atmospherically-fixed nitrogen on the early land surface that was probably too diffuse to
512 be a significant source of fixed nitrogen to the marine biosphere (Homann et al., 2018).

513

514 **5.2 Cavity-dwelling life**

515 Lens-shaped, laterally tapering cavities, up to tens of centimeters in width and <0.5 cm in height, frequently
516 occur beneath fossil microbial mat in intertidal deposits of the Saddleback Syncline (Fig. 14A; Homann et
517 al., 2016). The silicified cavities resemble gas-filled, fenestral hollows in modern coastal environments that
518 commonly form beneath cohesive, impermeable microbial mats and mat-bound sediments (Gerdes et al.,
519 2000; Schieber et al., 2007). Due to the presence of carbonaceous laminations and wisps these chert lenses
520 were initially interpreted as partially silicified epibenthic microstromatolites or thick mucilaginous mats
521 (Heubeck 2009; Gamper et al., 2011), however, Homann et al. (2016) reported the additional presence of
522 pendant columnar microstromatolites attached to the ceilings of former cavities and concluded that they
523 must have accreted downwards in an open void space of synsedimentary origin (Fig. 14B-E). This gravity-
524 oriented geometry and the downward-accretionary growth habit is well known from cavity-dwelling
525 microorganisms (coelobionts; Kobluk and James, 1979; Jakubowicz et al., 2014), which have also been
526 reported from synsedimentary cavities beneath microbial mats in sandstones of the Neoproterozoic Fortescue
527 Group in Australia (Rasmussen et al., 2009). In places, sub-circular to ovoid-shaped fenestrae (~500 µm in
528 diameter) that resemble trapped gas bubbles occur wedged between the carbonaceous laminae (Fig. 14C).
529 SEM observations of the cavity-filling cherts reveal the presence of: (1) polygonal structures after HF
530 etching for 28 days, interpreted as remnants of extracellular polymeric substance (EPS, Gamper et al.,
531 2012), and (2) a meshwork of interwoven filamentous molds of likely biogenic origin that is completely
532 embedded in the chert (Fig. 14F; unetched samples, Homann et al., 2016). The non-branching filaments
533 (0.3–0.5 µm in diameter, n = 180) display a subdivision in regularly spaced, ~2-µm- long, rod-shaped
534 segments and have a tubular morphology in cross section (Fig. 14G and H). Bulk carbon isotope
535 measurements of the chert-bearing sandstones show $\delta^{13}\text{C}_{\text{org}}$ values between -23.8‰ and -14.1‰ (mean =
536 -20.5‰, n = 15; Gamper et al., 2012), however, *in situ* measurements of the carbonaceous laminae within
537 the chert-cemented cavities yield $\delta^{13}\text{C}_{\text{org}}$ values ranging between -32.3‰ and -21.3‰ (mean = -26.5‰; n
538 = 12) that are probably more representative. These values are consistent with a purely chemotrophic or a
539 photosynthetic community of coelobionts and support the biogenicity of the oldest evidence for cavity-
540 dwelling life on Earth (Homann et al., 2016). Moreover, these findings support the view the cavities were
541 among the first ecological niches to have been occupied by early microbial communities.

542

543

544 **5.3 Organic-walled microfossils**

897
898
899
900
901
902
903
904
905
906
907
908
909
910
911
912
913
914
915
916
917
918
919
920
921
922
923
924
925
926
927
928
929
930
931
932
933
934
935
936
937
938
939
940
941
942
943
944
945
946
947
948
949
950
951
952

545 Carbonaceous spheroidal microstructures, 31–300 μm in diameter (mean=122 μm , n=98), have been
546 identified in bedded siltstones and shales from underground drill cores that were assigned to the Clutha
547 Formation and drilled 600m below the surface in the Agnes gold mine, Moodies Hills Block (Javaux et al.,
548 2010). The carbonaceous structures are visible in petrographic thin sections and resistant to extraction via
549 acid maceration (Fig. 15A-D). They show wrinkled and folded textures, a ~160-nm-thick wall with a
550 homogenous ultrastructure and were interpreted as flattened, hollow, and partially degraded, organic-walled
551 vesicles with preserved cell lumen (Fig. 15E-F; Javaux et al., 2010). Bulk carbon isotopes measurements
552 show a large spread in $\delta^{13}\text{C}_{\text{org}}$ values ranging between -16.4% and -28.3%, with an average of -22.4%
553 (n=22), but no difference in the $\delta^{13}\text{C}_{\text{org}}$ values between samples with and without microfossils has been
554 observed. Consequently, such bulk measurements might not be very useful in constraining the biogenicity
555 of the microstructures, however their carbonaceous composition and syngenetic origin is supported by
556 Raman microspectroscopy. Based on their taphonomy and for the Paleoproterozoic uncommonly large size,
557 Javaux et al. (2010) and Buick (2010). Javaux et al. (2010) concluded that the organic-walled microfossils
558 might either represent remnants of extinct prokaryotes, colonial envelopes of cyanobacteria, or even
559 eukaryotes. To unravel the biological affinity of these acritarchs remains the task for future investigations,
560 which should ideally also aim to identify the microstructures in outcrop samples in order to further constrain
561 their habitat and explore their possible relationship with the widespread, shallow-water microbial mats of
562 the Moodies Group.

564 **6. Discussion**

566 **6.1 Evidence of Paleoproterozoic life in the BGB and comparison to the PGBs**

567 Traces of ancient life in the BGB occur mainly confined to bedded, carbonaceous cherts of the Onverwacht
568 Group and the siliciclastic deposits of the Moodies Group. Preserved biosignatures in these deposits include
569 putative microfossils of filamentous, spheroidal, and lenticular shape, stromatolites, and microbial mats.
570 Filamentous microfossils occur very rarely in cherts of the Onverwacht Group but their biogenicity remains
571 equivocal (Walsh and Lowe, 1985; Walsh 1992, 2010). The rod-shaped filamentous molds preserved in
572 early silicified, syndepositional cavities of the Moodies Group resemble in shape and size microbial
573 filaments and also their depositional context, beneath intertidal microbial mats, supports a biogenic origin
574 (Homann et al., 2016). Spheroidal microstructures with carbonaceous walls, resembling coccoidal cells,
575 belong to the most common group of putative microfossils in the Onverwacht Group but the assessment of
576 their biogenicity is in most cases extremely challenging due to their simple, often symmetrical morphology
577 that can be easily generated abiogenetically in form of e.g. fluid inclusions, vesicles, and spheroidal
578 crystallites (Schopf and Walther 1983; Brasier et al., 2006). Solely, the spheroidal, cell-like objects reported

953
954
955
956
957
958
959
960
961
962
963
964
965
966
967
968
969
970
971
972
973
974
975
976
977
978
979
980
981
982
983
984
985
986
987
988
989
990
991
992
993
994
995
996
997
998
999
1000
1001
1002
1003
1004
1005
1006
1007
1008

579 by Glikson et al. (2008) from the Hooggenoeg Formation and the large, organic-walled spheroids described
580 by Javaux et al. (2010) from the Moodies Group have a well-established biogenicity. However, the
581 biological affinity of the latter and the reason for their unusually large size currently remains unknown.
582 Lenticular structures preserved in the Buck Reef Chert (Walsh 1992; Oehler et al., 2017) and probably also
583 other cherts of the upper Onverwacht Group (Pflug 1966, 1967; Pflug et al., 1969) belong to the earliest
584 reported and currently best studied microfossils in the BGB. Remains of these, likely planktonic,
585 microorganisms have also been reported from the 3.45 Ga Strelley Pool Formation and the ~3 Ga Farrel
586 Quartzite in the Pilbara Craton where their biogenicity is reasonably well established (e.g. Oehler et al.,
587 2009, 2017; Sugitani et al. 2007, 2010, 2013; House et al., 2013; Kozawa et al., 2018). The morphologically
588 similar specimens from Australia occur in the same depositional context and show strikingly similar mean
589 $\delta^{13}\text{C}_{\text{org}}$ values (-37.0% and -36.1%) in comparison to their South African counterparts with a mean $\delta^{13}\text{C}_{\text{org}}$
590 value of -37.3% (Oehler et al., 2017). Abiogenic models for the formation of similar-looking structures
591 derived from reworked vesicular volcanic glass exists (Wacey et al., 2018a, 2018b), however these pseudo-
592 fossils do not resemble the same morphological and microstructural complexity (Alleon et al., 2018;
593 Kozawa et al., 2018). Nevertheless, the occurrence of such pseudo-fossil examples highlights again the
594 paramount importance of detailed micro- and nanoscale analysis in the evaluation of the biogenicity of
595 putative microfossils. Additionally, future studies of microfossil-bearing cherts of the Onverwacht Group
596 should always be accompanied by detailed analysis of the stratigraphic context and depositional facies, in
597 combination with *in situ* geochemical analysis of the microfossils themselves and their encasing mineral
598 matrix.

599 Stromatolites, generally considered as the most ancient macroscopically-visible traces for life on Earth, are
600 surprisingly rare and currently not as well documented in the BGB in comparison to the PGBs, where the
601 oldest unequivocal biogenic examples occur preserved in the 3.45 Ga Strelley Pool Formation (Allwood,
602 et al 2006) and possibly also in the 3.48 Ga Dresser Formation (Fig. 16; Walter et al., 1980; Van
603 Kranendonk et al., 2008). However, the often morphological very simple, laminated, domal to conical
604 structures of Archean stromatolites can be easily confused with secondary abiogenic structures, especially
605 in the absence of indicative microfossils. A recent study of Allwood et al. (2018), highlighting the
606 importance of morphological analysis in combination with geochemistry at appropriate scales, serves as a
607 cautionary tale and strongly questions the biogenicity of previously reported putative stromatolites from
608 3.7 Ga old metacarbonate rocks of Greenland (Nutman et al., 2016). Compared to the greenstone belts in
609 the Pilbara region, the documented deposit of the BGB contain only minor evidence of early carbonate
610 environments, which is probably related to the predominance of volcanic and clastic deposition in
611 combination with high sedimentation rates that made the conditions for stromatolite formation less
612 favorable.

1009
1010
1011 613 The most widespread, pervasive, and probably also oldest trace of ancient life in the BGB are the remnants
1012 614 of shallow-water microbial mats and biofilms. Mat-like laminations occur in almost all black-and-white-
1013 615 banded, carbonaceous cherts of the Onverwacht Group (Walsh 1992), but only the examples reported from
1014 616 the 3.472 Ga Middle Marker (Hickman-Lewis, et al, 2018), the 3.416 Ga Buck Reef Chert (Walsh and
1015 617 Lowe, 1999; Tice and Lowe, 2004a, 2006a, b; Tice, 2009; Tice et al., 2011), and the 3.334 Ga Josefsdal
1016 618 Chert (Westall et al., 2011, 2006, 2011, 2015) are reasonably well studied to support their biogenic origin.
1017 619 Especially the mats and microfossils preserved in the up to 400-m-thick Buck Reef Chert represent a
1018 620 particularly widespread (~50 km along strike), well-preserved and -documented record of the Paleoproterozoic
1019 621 life. Besides the necessity to carefully reinvestigate more potentially microfossil- and mat-bearing
1020 622 carbonaceous cherts in the BGB it is also crucial to further support the already existing claims for early life
1021 623 from these units with more detailed geochemical analysis such as e.g. carbon, nitrogen, and sulphur isotope
1022 624 data. The microbial mats preserved in the tidal and fluvial sandstones and conglomerates of the 3.22 Ga
1023 625 Moodies Group are unique and currently not known from equivalent deposits from Australia (Fig. 16;
1024 626 Noffke et al., 2006; Heubeck, 2009; Gamper et al., 2012; Homann et al., 2015, 2018). The quality of
1025 627 preservation of the delicate carbonaceous mat laminae, distinct morphotypes, and mat-associated cavities
1026 628 in these coarse-grained and gravely siliciclastic deposits is truly exceptional and implies a rapid fossilization
1027 629 driven by early diagenetic silicification of the sediments (Heubeck 2009; Homann et al., 2015). The
1028 630 observed difference in the biogeochemical cycling of carbon and nitrogen in tidal marine and fluvial
1029 631 microbial mats from the Moodies Group (Homann et al., 2018) has demonstrated the potential of detailed
1030 632 geochemical analysis, which can give valuable insights in the different carbon fixation pathways and
1031 633 ultimately helps to constrain the metabolism(s) of the mat-building microbial communities and should
1032 634 consequently also be applied more extensively to the mats preserved in the Onverwacht Group.
1033
1034
1035
1036
1037
1038
1039
1040
1041
1042
1043
1044

1045 636 **6.2 Habitats and paleoecology**

1046 637 Evidence for Paleoproterozoic life in the BGB have been reported from a wide range of paleoenvironments
1047 638 including shallow marine (e.g. Byerly et al., 1986; Tice and Lowe, 2004a; Heubeck 2009; Homann et al.,
1048 639 2015), fluvial (Homann et al., 2018), hydrothermal (Glikson et al., 2008; Westall et al., 2015), and possibly
1049 640 planktonic settings (Walsh 1992; Oehler et al., 2017), as well as from cryptic cavities in the shallow
1050 641 subsurface of intertidal deposits (Homann et al., 2016). Due to the general restriction of microbial mats to
1051 642 shallow-water, photic zone paleoenvironments of the BGB, the common notion is that they were at least in
1052 643 part composed of photosynthetic microbial communities and already had a high level of UV radiation
1053 644 tolerance, while the microorganisms thriving in a hydrothermal context or in cavities were likely dominated
1054 645 by chemotrophic communities. Nearly all of these early microbial communities must have been severely
1055 646 affected by distant impacts of large asteroids (20 to 50 km in diameter), which occurred between 3.470 Ga
1056
1057
1058
1059
1060
1061
1062
1063
1064

1065
1066
1067 647 and 3.225 Ga and are recorded in the BGB deposits by eight known ejecta layers (Fig. 2; Lowe and Byerly,
1068 648 1986, 2018; Lowe et al., 1989). Besides impact-generated tsunamis it has been proposed that some of these
1069 649 catastrophic events might have been large enough to cause partial boiling and sterilization of the oceans
1070 650 and possibly triggered mass extinctions of low-temperature microbes, including most photosynthetic
1071 651 microorganisms (Sleep et al., 1989; Lowe and Byerly, 2015). The question of how exactly early life
1072 652 managed to survive these events or if the global ecosystem got entirely destroyed and biogenesis was reset
1073 653 currently remains open.

1077 654 The Moodies Group ecosystem was particularly diverse, advanced, and well-adapted and includes large
1078 655 spheroidal microfossils, Earth's earliest evidence of cavity-dwelling microbes (coelobionts), widespread
1079 656 intertidal tufted microbial mats, laterally traceable for 15 km in a ~1000 m-thick succession, as well as
1080 657 erosion-resistant fluvial microbial mats. The latter represent the oldest known direct fossil evidence for
1081 658 terrestrial life on the continental surface and are ~500 Ma older than ~2.7 Ga old fluvio-lacustrine
1082 659 stromatolites and coelobionts preserved in the Fortescue Group (Tumbiana and Hardey Formation,
1083 660 Australia; Buick, 1992; Awramik and Buchheim, 2009; Rasmussen et al., 2009; Coffey et al., 2013) and
1084 661 fluvial stromatolites documented in the Ventersdorp Supergroup (South Africa; Buck, 1980). Based on the
1085 662 apparent morphological similarities between the shallow-marine microbial mats of the Moodies Group and
1086 663 modern cyanobacterial mats such as e.g. macroscopic tufts, evidence for gas production and accumulation
1087 664 in bubbles and domes, and their widespread occurrence and presumably fast growth rate, it has been
1088 665 proposed that they were perhaps build by ancestral cyanobacteria (Homann et al., 2015). A recent molecular
1089 666 clock study by Cardona et al. (2018) supports this interpretation and suggest that a primordial photosystem
1090 667 capable of oxidizing water to oxygen could have formed before the most recent common ancestor of
1091 668 cyanobacteria. Additionally, also the unusually large size of the organic-walled microfossils reported by
1092 669 Javaux et al. (2010) indirectly suggests the requirement and the availability of oxygen at 3.22 Ga, although
1093 670 no unequivocal geochemical signs for the local presence of free oxygen have been found so far in the
1094 671 Moodies Group.

1103 672

1105 673 **7. Conclusions**

1106 674 The deposits of the Barberton Greenstone Belt host a large variety of convincing macro- and microscopic,
1107 675 as well as geochemical evidence for early microbial life. It was predominantly thriving in shallow marine
1108 676 environments in the photic zone but started to spread out to colonize fluvial habitats in emerged continental
1109 677 surface environments and also occupied the first ecological niches, such as subsurface cavities. Traces of
1110 678 ancient life in the BGB occur scattered throughout the entire stratigraphy confined to carbonaceous cherts
1111 679 of the Onverwacht Group and siliciclastic deposits of the Moodies Group. However, their identification is
1112 680 sometimes solely based on morphological attributes and not always accompanied by detailed and systematic

1116
1117
1118
1119
1120

1121
1122
1123 681 geochemical analysis at appropriate scales, which should be improved in future investigations. Due to their
1124 682 wealth of remarkably preserved microbial mats and microfossils, consistent lateral exposure for several
1125 683 tens of kilometers and thick stratigraphy, especially the deposits of the 3.416 Ga Buck Reef Chert and the
1127 684 sandstones of the 3.22 Ga Moodies Group represent a unique window into a diverse Paleoproterozoic
1128 685 biosphere.
1130 686 Based on its universal and outstanding geological and paleobiological value the Barberton-Makhonjwa
1131 687 Mountains were inscribed in the UNESCO World Heritage Site register in 2018, which will ultimately help
1132 688 to protect these exceptional outcrops for future studies of Earth's early evolution.
1134 689
1135 690

1137 691 **Acknowledgements**

1138 692 This work was greatly supported by LabexMER ANR-10-LABX-19 and Prestige COFUND-GA-2013-
1140 693 609102 to M.H. Amongst many others, the author would especially like to thank Maud Walsh, Gary Byerly,
1141 694 Don Lowe, Christoph Heubeck, Dorothy Oehler, Wlady Altermann, and Andrew Knoll for their helpful
1143 695 comments. I am also indebted to Stefan Lalonde and Claire Earlie for useful discussions and comments on
1144 696 an earlier version of the manuscript.
1146 697

1147 698

1148 699

1150 700 **References**

1151 701

1153 702 Ader, M., Thomazo, C., Sansjofre, P., Busigny, V., Papineau, D., Laffont, R., Cartigny, P., Halverson,
1154 703 G.P., 2016. Interpretation of the nitrogen isotopic composition of Precambrian sedimentary rocks:
1156 704 Assumptions and perspectives. *Chem. Geol.* 429, 93–110.
1157 705 <https://doi.org/10.1016/j.chemgeo.2016.02.010>

1159 706 Alleon, J., Bernard, S., Le Guillou, C., Beyssac, O., Sugitani, K., Robert, F., 2018. Chemical nature of the
1160 707 3.4 Ga Strelley Pool microfossils. *Geochemical Perspect. Lett.* 37–42.
1162 708 <https://doi.org/10.7185/geochemlet.1817>

1163 709 Allwood, A.C., Rosing, M.T., Flannery, D.T., Hurowitz, J.A., Heirwegh, C.M., 2018. Reassessing
1165 710 evidence of life in 3,700-million-year-old rocks of Greenland. *Nature*.
1166 711 <https://doi.org/10.1038/s41586-018-0610-4>

1168 712 Allwood, A.C., Walter, M.R., Kamber, B.S., Marshall, C.P., Burch, I.W., 2006. Stromatolite reef from the
1169 713 Early Archaean era of Australia. *Nature* 441, 714–718. <https://doi.org/10.1038/nature04764>

1171 714 Altermann, W., 2001. The oldest fossils of Africa – a brief reappraisal of reports from the Archean. *J.*

1172

1173

1174

1175

1176

1177
1178
1179 715 African Earth Sci. 33, 427–436. [https://doi.org/10.1016/S0899-5362\(01\)00089-6](https://doi.org/10.1016/S0899-5362(01)00089-6)
1180 716 Anhaeusser, C.R., 1976. The geology of the sheba hills area of the Barberton Mountain Land, South
1181 Africa with particular reference to the Eureka Syncline. *Trans. Geol. Soc. S. Africa* 79, 253–280.
1182 717
1183 718 Armstrong, R.A., Compston, W., de Wit, M., Williams, I.S., 1990. The stratigraphy of the 3.5–3.2 Ga
1184 Barberton Greenstone Belt revisited: a single zircon ion microprobe study. *Earth Planet. Sci. Lett.*
1185 719 101, 90–106.
1186 720
1187 721 Awramik, S.M., 1992. The oldest records of photosynthesis. *Photosynth. Res.* 33, 75–89.
1188 722 <https://doi.org/10.1007/BF00039172>
1189 723 Awramik, S.M., Buchheim, H.P., 2009. A giant, Late Archean lake system: The Meentheena Member
1190 (Tumbiana Formation; Fortescue Group), Western Australia. *Precambrian Res.* 174, 215–240.
1191 724 <https://doi.org/10.1016/j.precamres.2009.07.005>
1192 725
1193 726 Banerjee, N.R., Simonetti, A., Banerjee, N.R., Sciences, E., Ontario, W., Na, O., 2007. Direct dating of
1194 Archean microbial ichnofossils Direct dating of Archean microbial ichnofossils.
1195 727 <https://doi.org/10.1130/G23534A.1>
1196 728
1197 729 Barghoorn, E.S., 1971. The oldest fossils. *Sci. Am.* 224, 30–43.
1200 730 Barghoorn, E.S., Schopf, J.W., 1966. Microorganisms Three Billion Years Old from the Precambrian of
1201 South Africa. *Science (80-)*. 152, 758–763. <https://doi.org/10.1126/science.152.3723.758>
1202 731
1203 732 Bosak, T., Bush, J.W.M., Flynn, M.R., Liang, B., Ono, S., Petroff, a. P., Sim, M.S., 2010. Formation and
1204 stability of oxygen-rich bubbles that shape photosynthetic mats. *Geobiology* 8, 45–55.
1205 733 <https://doi.org/10.1111/j.1472-4669.2009.00227.x>
1206 734
1207 735 Bose, S., Chafetz, H.S., 2009. Topographic control on distribution of modern microbially induced
1208 sedimentary structures (MISS): A case study from Texas coast. *Sediment. Geol.* 213, 136–149.
1209 736 <https://doi.org/10.1016/j.sedgeo.2008.11.009>
1210 737
1211 738 Brasier, M., McLoughlin, N., Green, O., Wacey, D., 2006. A fresh look at the fossil evidence for early
1212 Archaeal cellular life. *Philos. Trans. R. Soc. Lond. B. Biol. Sci.* 361, 887–902.
1213 739 <https://doi.org/10.1098/rstb.2006.1835>
1214 740
1215 741 Brooks, J., Muir, M.D., Shaw, G., 1973. Chemistry and Morphology of Precambrian Microorganisms.
1216 742 *Nature* 244, 215–217. <https://doi.org/10.1038/244215a0>
1217 743 Brooks, J., Shaw, G., 1971. Evidence for Life in the Oldest Known Sedimentary Rocks—the Onverwacht
1218 Series Chert, Swaziland System of Southern Africa. *Grana* 11, 1–8.
1219 744 <https://doi.org/10.1080/00173137109427403>
1220 745
1221 746 Buck, S.G., 1980. Stromatolite and ooid deposits within the fluvial and lacustrine sediments of the
1222 Precambrian Ventersdorp Supergroup of South Africa. *Precambrian Res.* 12, 311–330.
1223 747 [https://doi.org/10.1016/0301-9268\(80\)90033-9](https://doi.org/10.1016/0301-9268(80)90033-9)
1224 748
1225
1226
1227
1228
1229
1230
1231
1232

1233
1234
1235 749 Buick, R., 2010. Early life: Ancient acritarchs. *Nature* 463, 885–886. <https://doi.org/10.1038/463885a>
1236 750 Buick, R., 1992. The antiquity of oxygenic photosynthesis: evidence from stromatolites in sulphate-
1237 deficient Archean lakes. *Science* (80-.). 255, 74–77. <https://doi.org/10.1126/science.11536492>
1238 751
1239 752 Byerly, G.R., 1999. Komatiites of the Mendon Formation: Late-stage ultramafic volcanism in the
1240 Barberton Greenstone Belt, in: Lowe, D.R., Byerly, G.R. (Eds.), *Geologic Evolution of the*
1241 753 *Barberton Greenstone Belt, South Africa*. Geological Society of America, p. 0.
1242 754
1243 755 <https://doi.org/10.1130/0-8137-2329-9.189>
1244
1245 756 Byerly, G.R., Lowe, D.R., Heubeck, C., 2019. Geologic Evolution of the Barberton Greenstone Belt—A
1246 Unique Record of Crustal Development, Surface Processes, and Early Life 3.55–3.20 Ga, in: *Earth’s*
1247 757 *Oldest Rocks*. Elsevier, pp. 569–613. <https://doi.org/10.1016/B978-0-444-63901-1.00024-1>
1248 758
1249 759 Byerly, G.R., Lowe, D.R., Walsh, M.M., 1986. Stromatolites from the 3,300–3,500-Myr Swaziland
1250 Supergroup, Barberton Mountain Land, South Africa. *Nature* 319, 489–491.
1251 760
1252 761 Byerly, G.R., Palmer, M.R., 1991. Tourmaline mineralization in the Barberton greenstone belt, South
1253 Africa: early Archean metasomatism by evaporite-derived boron. *Contrib. to Mineral. Petrol.* 107,
1254 762 387–402. <https://doi.org/10.1007/BF00325106>
1255 763
1256 764 Cardona, T., Sánchez-Baracaldo, P., Rutherford, A.W., Larkum, A.W., 2018. Early Archean origin of
1257 Photosystem II. *Geobiology* 4, e00548. <https://doi.org/10.1111/gbi.12322>
1258 765
1259 766 Coffey, J.M., Flannery, D.T., Walter, M.R., George, S.C., 2013. Sedimentology, stratigraphy and
1260 geochemistry of a stromatolite biofacies in the 2.72Ga Tumbiana Formation, Fortescue Group,
1261 767 Western Australia. *Precambrian Res.* 236, 282–296.
1262 768
1263 <https://doi.org/10.1016/j.precamres.2013.07.021>
1264 769
1265 770 De Ronde, C.E.J., De Wit, M.J., 1994. Tectonic history of the Barberton greenstone belt, South Africa:
1266 490 million years of Archean crustal evolution. *Tectonics* 13, 983–1005.
1267 771
1268 772 <https://doi.org/10.1029/94TC00353>
1269
1270 773 De Ronde, C.E.J., Kamo, S.L., 2000. An Archean arc-arc collisional event: A short-lived (ca 3 Myr)
1271 774 episode, Weltevreden area, Barberton greenstone belt, South Africa. *J. African Earth Sci.* 30, 219–
1272 248. [https://doi.org/10.1016/S0899-5362\(00\)00017-8](https://doi.org/10.1016/S0899-5362(00)00017-8)
1273 775
1274 776 De Wit, M.J., Furnes, H., R., 2011. Geology and tectonostratigraphy of the Onverwacht Suite, Barberton
1275 Greenstone Belt. *Precambrian Res.* 186, 28–50.
1276 777
1277 778 de Wit, M.J., Hart, R., Martin, A., Abbott, P., 1982. Archean abiogenic and probable biogenic structures
1278 associated with mineralized hydrothermal vent systems and regional metasomatism, with
1279 779 implications for greenstone belt studies. *Econ. Geol.* 77, 1783–1802.
1280 780
1281 781 <https://doi.org/10.2113/gsecongeo.77.8.1783>
1282
1283 782 Engel, A.E.J., Nagy, B., Nagy, L.A., Engel, C.G., Kremp, G.O.W., Drew, C.M., 1968. Alga-Like Forms
1284
1285
1286
1287
1288

1289
1290
1291 783 in Onverwacht Series, South Africa: Oldest Recognized Lifelike Forms on Earth. *Science* (80-.).
1292 784 161, 1005–1008. <https://doi.org/10.1126/science.161.3845.1005>
1293
1294 785 Eriksson, K.A., 1979. Marginal marine depositional processes from the Archaean Moodies Group,
1295 786 Barberton Mountain Land; South Africa: Evidence and significance. *Precambrian Res.* 8, 153–182.
1296
1297 787 Eriksson, K.A., 1977. Tidal deposits from the Archaean Moodies Group, Barberton Mountain Land,
1298 788 South Africa. *Sediment. Geol.* 18, 257–281.
1299
1300 789 Fliegel, D., Simonetti, A., Furnes, H., 2010. In-situ dating of the Earth ' s oldest trace fossil.
1301 790 <https://doi.org/10.1016/j.epsl.2010.09.008>
1302
1303 791 Furnes, H., 2004. Early Life Recorded in Archean Pillow Lavas. *Science* (80-.). 304, 578–581.
1304 792 <https://doi.org/10.1126/science.1095858>
1305
1306 793 Furnes, H., Banerjee, N.R., Staudigel, H., Muehlenbachs, K., McLoughlin, N., Wit, M. De, Kranendonk,
1307 794 M. Van, 2007. Comparing petrographic signatures of bioalteration in recent to Mesoarchean pillow
1308 795 lavas : Tracing subsurface life in oceanic igneous rocks 158, 156–176.
1309
1310 796 <https://doi.org/10.1016/j.precamres.2007.04.012>
1311
1312 797 Gamper, A., Heubeck, C., Demske, D., Hoehse, M., 2012. Composition and Microfacies of Archean
1313 798 Microbial Mats (Moodies Group, ca. 3.22 Ga, South Africa), in: Noffke, N., Chafetz, H.S. (Eds.),
1314 799 Microbial Mats in Siliclastic Depositional Systems Through Time. *SEPM (Society for Sedimentary*
1315
1316 800 *Geology)*, Tulsa, pp. 65–74. <https://doi.org/10.2110/sepmsp.101.065>
1317 801 Gerdes, G., 2007. Structures Left by Modern Microbial Mats in Their Host Sediments, in: Schieber, J.,
1318 802 Bose, P.K., Eriksson, P., Banerjee, S., Sarkar, S., Altermann, W., Catuneanu, O. (Eds.), *Atlas of*
1319 803 *Microbial Mat Features Preserved within the Siliciclastic Rock Record.* Elsevier, Amsterdam, pp. 5–
1320 804 38. [https://doi.org/10.1016/S1574-1966\(07\)02001-9](https://doi.org/10.1016/S1574-1966(07)02001-9)
1321
1322 805 Gerdes, G., Klenke, T., Noffke, N., 2000. Microbial signatures in peritidal siliciclastic sediments: a
1324 806 catalogue. *Sedimentology* 47, 279–308.
1325
1326 807 Glikson, M., Duck, L.J., Golding, S.D., Hofmann, A., Bolhar, R., Webb, R., Baiano, J.C.F., Sly, L.I.,
1327 808 2008. Microbial remains in some earliest Earth rocks: Comparison with a potential modern
1328
1329 809 analogue. *Precambrian Res.* 164, 187–200. <https://doi.org/10.1016/j.precamres.2008.05.002>
1330
1331 810 Grosch, E.G., McLoughlin, N., 2014. Reassessing the biogenicity of Earth's oldest trace fossil with
1332 811 implications for biosignatures in the search for early life. *Proc. Natl. Acad. Sci.* 111, 8380–8385.
1333 812 <https://doi.org/10.1073/pnas.1402565111>
1334
1335 813 Hall, A.L., 1918. The geology of the Barberton gold mining district. *Geol. Surv. South Africa Mem.* 9,
1336 814 347.
1337
1338 815 Heinrichs, T.K., Reimer, T., 1977. Geology and tectonostratigraphy of the Onverwacht Suite, Barberton
1339 816 greenstone belt, South Africa. *Econ. Geol.* 72, 1426–1441.
1340
1341
1342
1343
1344

1345
1346
1347 817 Heubeck, C., 2009. An early ecosystem of Archean tidal microbial mats (Moodies Group, South Africa,
1348 818 ca. 3.2 Ga). *Geology* 37, 931–934. <https://doi.org/10.1130/G30101A.1>
1349
1350 819 Heubeck, C., Bläsing, S., Grund, M., Drabon, N., Homann, M., Nabhan, S., 2016. Geological constraints
1351 820 on Archean (3.22 Ga) coastal-zone processes from the Dycedale Syncline, Barberton Greenstone
1352 821 Belt. *South African J. Geol.* 119, 495–518. <https://doi.org/10.2113/gssajg.119.3.495>
1353
1354 822 Heubeck, C., Engelhardt, J., Byerly, G.R., Zeh, A., Sell, B., Luber, T., Lowe, D.R., 2013. Timing of
1355 823 deposition and deformation of the Moodies Group (Barberton Greenstone Belt, South Africa): Very-
1356 824 high-resolution of Archaean surface processes. *Precambrian Res.* 231, 236–262.
1357 825 <https://doi.org/10.1016/j.precamres.2013.03.021>
1358
1359 826 Heubeck, C., Lowe, D.R., 1999. Sedimentary petrography and provenance of the Archean Moodies Grou,
1360 827 Barberton Greenstone Belt, in: Lowe, D.R., Byerly, G.R. (Eds.), *Geologic Evolution of the*
1361 828 *Barberton Greenstone Belt, South Africa*. Geological Society of America Special Paper 329, pp.
1362 829 259–286.
1363
1364 830 Heubeck, C., Lowe, D.R., 1994a. Depositional and tectonic setting of the Archean Moodies Group,
1365 831 Barberton greenstone belt, South Africa. *Precambrian Res.* 68, 257–290.
1366
1367 832 Heubeck, C., Lowe, D.R., 1994b. Late syndepositional deformation and detachment tectonics in the
1368 833 Barberton Greenstone Belt, South Africa. *Tectonics* 13, 1514–1536.
1369
1370 834 Hickman-Lewis, K., Cavalazzi, B., Foucher, F., Westall, F., 2018. Most ancient evidence for life in the
1371 835 Barberton greenstone belt: Microbial mats and biofabrics of the ~3.47 Ga Middle Marker horizon.
1372 836 *Precambrian Res.* 312, 45–67. <https://doi.org/10.1016/j.precamres.2018.04.007>
1373
1374 837 Hickman-Lewis, K., Westall, F., Cavalazzi, B., 2019. Traces of Early Life From the Barberton
1375 838 Greenstone Belt, South Africa, in: *Earth's Oldest Rocks*. Elsevier B.V., pp. 1029–1058.
1376 839 <https://doi.org/10.1016/B978-0-444-63901-1.00042-3>
1377
1378 840 Hofmann, A., 2005. The geochemistry of sedimentary rocks from the Fig Tree Group, Barberton
1379 841 greenstone belt: Implications for tectonic, hydrothermal and surface processes during mid-Archaean
1380 842 times. *Precambrian Res.* 143, 23–49. <https://doi.org/10.1016/j.precamres.2005.09.005>
1381
1382 843 Hofmann, A., Bolhar, R., 2007. Carbonaceous cherts in the Barberton greenstone belt and their
1383 844 significance for the study of early life in the Archean record. *Astrobiology* 7, 355–388.
1384 845 <https://doi.org/10.1089/ast.2005.0288>
1385
1386 846 Hofmann, A., Harris, C., 2008. Silica alteration zones in the Barberton greenstone belt : A window into
1387 847 subsea floor processes 3.5 – 3.3 Ga ago. *Chem. Geol.* 257, 221–239.
1388 848 <https://doi.org/10.1016/j.chemgeo.2008.09.015>
1389
1390 849 Homann, M., Heubeck, C., Airo, A., Tice, M.M., 2015. Morphological adaptations of 3.22 Ga-old tufted
1391 850 microbial mats to Archean coastal habitats (Moodies Group, Barberton Greenstone Belt, South
1392
1393
1394
1395
1396
1397
1398
1399
1400

1401
1402
1403 851 Africa). *Precambrian Res.* 266, 47–64. <https://doi.org/10.1016/j.precamres.2015.04.018>
1404 852 Homann, M., Heubeck, C., Bontognali, T.R.R., Bouvier, A.S., Baumgartner, L.P., Airo, A., 2016.
1405 853 Evidence for cavity-dwelling microbial life in 3.22 Ga tidal deposits. *Geology* 44, 51–54.
1406 854 <https://doi.org/10.1130/G37272.1>
1407 855 Homann, M., Sansjofre, P., Van Zuilen, M., Heubeck, C., Gong, J., Killingsworth, B., Foster, I.S., Airo,
1408 856 A., Van Kranendonk, M.J., Ader, M., Lalonde, S. V, 2018. Microbial life and biogeochemical
1409 857 cycling on land 3,220 million years ago. *Nat. Geosci.* 11, 665–671. [https://doi.org/10.1038/s41561-](https://doi.org/10.1038/s41561-018-0190-9)
1410 858 018-0190-9
1411 859 House, C.H., Oehler, D.Z., Sugitani, K., Mimura, K., 2013. Carbon isotopic analyses of ca. 3.0 Ga
1412 860 microstructures imply planktonic autotrophs inhabited earth’s early oceans. *Geology* 41, 651–654.
1413 861 <https://doi.org/10.1130/G34055.1>
1414 862 Jahnert, R.J., Collins, L.B., 2013. Controls on microbial activity and tidal flat evolution in Shark Bay,
1415 863 Western Australia. *Sedimentology* 60, 1071–1099. <https://doi.org/10.1111/sed.12023>
1416 864 Jakubowicz, M., Berkowski, B., Belka, Z., 2014. Cryptic coral-crinoid “hanging gardens” from the
1417 865 Middle Devonian of southern Morocco. *Geology* 42, 119–122. <https://doi.org/10.1130/G35217.1>
1418 866 Javaux, E.J., Marshall, C.P., Bekker, A., 2010. Organic-walled microfossils in 3.2-billion-year-old
1419 867 shallow-marine siliciclastic deposits. *Nature* 463, 934–8. <https://doi.org/10.1038/nature08793>
1420 868 Karkhanis, S.N., 1977. Artifacts produced by chemical processing of samples for micropalaeontology and
1421 869 organic geochemistry - a note of caution. *Precambrian Res.* 4, 229–236.
1422 870 [https://doi.org/10.1016/0301-9268\(77\)90015-8](https://doi.org/10.1016/0301-9268(77)90015-8)
1423 871 Knauth, L.P., Lowe, D.R., 2003. High Archean climatic temperature inferred from oxygen isotope
1424 872 geochemistry of cherts in the 3.5 Ga Swaziland Supergroup, South Africa. *Bull. Geol. Soc. Am.*
1425 873 115, 566–580. [https://doi.org/10.1130/0016-7606\(2003\)115<0566:HACTIF>2.0.CO;2](https://doi.org/10.1130/0016-7606(2003)115<0566:HACTIF>2.0.CO;2)
1426 874 Knoll, A.H., Barghoorn, E.S., 1977. Archean Microfossils Showing Cell Division from the Swaziland
1427 875 System of South Africa. *Science* (80-.). 198, 396–398.
1428 876 <https://doi.org/10.1126/science.198.4315.396>
1429 877 Kobluk, D.R., James, N.P., 1979. Cavity-dwelling organisms in Lower Cambrian patch reefs from
1430 878 southern Labrador. *Lethaia* 12, 193–218. <https://doi.org/10.1111/j.1502-3931.1979.tb00997.x>
1431 879 Kozawa, T., Sugitani, K., Oehler, D.Z., House, C.H., Saito, I., Watanabe, T., Gotoh, T., 2018. Early
1432 880 Archean planktonic mode of life: Implications from fluid dynamics of lenticular microfossils.
1433 881 *Geobiology* 1–14. <https://doi.org/10.1111/gbi.12319>
1434 882 Kremer, B., Kaźmierczak, J., 2017. Cellularly preserved microbial fossils from ~3.4 Ga deposits of South
1435 883 Africa: A testimony of early appearance of oxygenic life? *Precambrian Res.* 295, 117–129.
1436 884 <https://doi.org/10.1016/j.precamres.2017.04.023>
1437
1438
1439
1440
1441
1442
1443
1444
1445
1446
1447
1448
1449
1450
1451
1452
1453
1454
1455
1456

1457
1458
1459 885 Kröner, A., Byerly, G.R., Lowe, D.R., 1991. Chronology of early Archaean granite-greenstone evolution
1460 886 in the Barberton Mountain Land , South Africa , based on precise dating by single zircon
1461
1462 887 evaporation. *Earth Planet. Sci. Lett.* 103, 41–54.
1463 888 Kröner, A., Hegner, E., Wendt, J.I., Byerly, G.R., 1996. The oldest part of the Barberton granitoid-
1464
1465 889 greenstone terrain, South Africa: evidence for crust formation between 3.5 and 3.7 Ga. *Precambrian*
1466 890 *Res.* 78, 105–124. [https://doi.org/10.1016/0301-9268\(95\)00072-0](https://doi.org/10.1016/0301-9268(95)00072-0)
1467
1468 891 Lamb, S., Paris, I., 1988. Post-onverwacht group stratigraphy in the SE part of the Archaean Barbeton
1469 892 greenstone belt. *J. African Earth Sci. (and Middle East)* 7, 285–306. [https://doi.org/10.1016/0899-](https://doi.org/10.1016/0899-5362(88)90074-7)
1470 893 [5362\(88\)90074-7](https://doi.org/10.1016/0899-5362(88)90074-7)
1471
1472 894 Lanier, W.P., Lowe, D.R., 1982. Sedimentology of the Middle Marker (3.4 Ga), Onverwacht Group,
1473 895 Transvaal, South Africa. *Precambrian Res.* 18, 237–260. [https://doi.org/10.1016/0301-](https://doi.org/10.1016/0301-9268(82)90012-2)
1474 896 [9268\(82\)90012-2](https://doi.org/10.1016/0301-9268(82)90012-2)
1475
1476 897 Lepot, K., Williford, K.H., Ushikubo, T., Sugitani, K., Mimura, K., Spicuzza, M.J., Valley, J.W., 2013.
1477 898 Texture-specific isotopic compositions in 3 . 4 Gyr old organic matter support selective preservation
1478 899 in cell-like structures. *Geochim. Cosmochim. Acta* 112, 66–86.
1480 900 <https://doi.org/10.1016/j.gca.2013.03.004>
1481
1482 901 Lowe, D.R., 1999a. Geologic evolution of the Barberton Greenstone Belt and vicinity, in: Lowe, D.R.,
1483 902 Byerly, G. (Ed.), *Special Paper 329: Geologic Evolution of the Barberton Greenstone Belt, South*
1484 903 *Africa. Geological Society of America*, pp. 287–312. <https://doi.org/10.1130/0-8137-2329-9.287>
1485
1486 904 Lowe, D.R., 1999b. Petrology and sedimentology of cherts and related silicified sedimentary rocks in the
1487 905 Swaziland Supergroup, in: Lowe, D.R., Byerly, G.R. (Eds.), *Geologic Evolution of the Barberton*
1488 906 *Greenstone Belt, South Africa. Geological Society of America*, p. 0. [https://doi.org/10.1130/0-8137-](https://doi.org/10.1130/0-8137-2329-9.83)
1489 907 [2329-9.83](https://doi.org/10.1130/0-8137-2329-9.83)
1490
1491 908 Lowe, D.R., 1999c. Shallow-water sedimentation of accretionary lapilli-bearing strata of the Msauli
1492 909 Chert: Evidence of explosive hydromagmatic komatiitic volcanism, in: *Special Paper 329: Geologic*
1493 910 *Evolution of the Barberton Greenstone Belt, South Africa. Geological Society of America*, pp. 213–
1494 911 232. <https://doi.org/10.1130/0-8137-2329-9.213>
1495
1496 912 Lowe, D.R., 1994. Accretionary history of the Archean Barberton greenstone belt (3.55-3.22 Ga),
1497 913 southern Africa. *Geology* 22, 1099–1102.
1498
1499 914 Lowe, D.R., Byerly, G.R., 2018. The terrestrial record of Late Heavy Bombardment. *New Astron. Rev.*
1500 915 81, 39–61. <https://doi.org/10.1016/j.newar.2018.03.002>
1501
1502 916 Lowe, D.R., Byerly, G.R., 2015. Geologic record of partial ocean evaporation triggered by giant asteroid
1503 917 impacts, 3.29-3.23 billion years ago. *Geology* 43, 535–538. <https://doi.org/10.1130/G36665.1>
1504
1505 918 Lowe, D.R., Byerly, G.R., 2007. Ironstone bodies of the Barberton greenstone belt, South Africa:
1506
1507
1508
1509
1510
1511
1512

1513
1514
1515 919 Products of a Cenozoic hydrological system, not Archean hydrothermal vents! *GSA Bull.* 119, 65–
1516 920 87. <https://doi.org/10.1130/b25997.1>
1517
1518 921 Lowe, D.R., Byerly, G.R., 1999. Stratigraphy of the west-central part of the Barberton Greenstone Belt,
1519 922 South Africa, in: Lowe, D.R., Byerly, G.R. (Eds.), *Geologic Evolution of the Barberton Greenstone*
1520 923 *Belt, South Africa. Geological Society of America Special Paper 329*, pp. 1–36.
1522 924 Lowe, D.R., Byerly, G.R., 1986. Early Archean silicate spherules of probable impact origin, South Africa
1523 925 and Western Australia. *Geology* 14, 83. [https://doi.org/10.1130/0091-](https://doi.org/10.1130/0091-7613(1986)14<83:EASSOP>2.0.CO;2)
1525 926 [7613\(1986\)14<83:EASSOP>2.0.CO;2](https://doi.org/10.1130/0091-7613(1986)14<83:EASSOP>2.0.CO;2)
1526 927 Lowe, D.R., Byerly, G.R., Asaro, F., Kyte, F.J., 1989. Geological and Geochemical Record of 3400-
1527 928 Million-Year-Old Terrestrial Meteorite Impacts. *Science* (80-.). 245, 959–962.
1529 929 <https://doi.org/10.1126/science.245.4921.959>
1530
1531 930 Lowe, D.R., Byerly, G.R., Heubeck, C., 2012. Geologic Map of the west-central Barberton Greenstone
1532 931 Belt, in: South Africa, Scale 1:25,000. Geological Society of America Map and Chart Series No.
1533 932 103, Boulder. <https://doi.org/10.1130/2012.MCH103>
1534 933 Lowe, D.R., Knauth, L.P., 1977. Sedimentology of the Onverwacht Group (3.4 Billion Years), Transvaal,
1535 934 South Africa, and Its Bearing on the Characteristics and Evolution of the Early Earth. *J. Geol.* 85,
1536 935 699–723. <https://doi.org/10.1086/628358>
1537 936 Lowe, D.R., Worrell, G.F., 1999. Sedimentology, mineralogy, and implications of silicified evaporites in
1538 937 the Kromberg Formation, Barberton Greenstone Belt, South Africa, in: *Special Paper 329: Geologic*
1539 938 *Evolution of the Barberton Greenstone Belt, South Africa. Geological Society of America*, pp. 167–
1540 939 188. <https://doi.org/10.1130/0-8137-2329-9.167>
1541 940 Mcloughlin, N., Grosch, E.G., Kilburn, M.R., Wacey, D., 2012. Sulfur isotope evidence for a
1542 941 Paleoproterozoic subseafloor biosphere, Barberton, South Africa 1031–1035.
1543 942 <https://doi.org/10.1130/G33313.1>
1544 943 Muir, M.D., Grant, P.R., 1976. Micropalaeontological evidence from the Onverwacht Group, South
1545 944 Africa, in: Windley, B.. (Ed.), *The Early History of the Earth*. John Wiley & Sons, New York, pp.
1546 945 595–608.
1547 946 Muir, M.D., Hall, D.O., 1974. Diverse microfossils in Precambrian Onverwacht group rocks of South
1548 947 Africa. *Nature* 252, 376–378. <https://doi.org/10.1038/252376a0>
1549 948 Nabhan, S., Lubber, T., Scheffler, F., Heubeck, C., 2016a. Climatic and geochemical implications of
1550 949 Archean pedogenic gypsum in the Moodies Group (~3.2 Ga), Barberton Greenstone Belt, South
1551 950 Africa. *Precambrian Res.* 275, 119–134. <https://doi.org/10.1016/j.precamres.2016.01.011>
1552 951 Nabhan, S., Wiedenbeck, M., Milke, R., Heubeck, C., 2016b. Biogenic overgrowth on detrital pyrite in
1553 952 ca. 3.2 Ga Archean paleosols. *Geology* 44, 763–766. <https://doi.org/10.1130/G38090.1>
1554
1555
1556
1557
1558
1559
1560
1561
1562
1563
1564
1565
1566
1567
1568

1569
1570
1571 953 Nagy, B., Nagy, L.A., 1969. Early Pre-Cambrian Onverwacht Microstructures : Possibly the Oldest
1572 954 Fossils on Earth? *Nature* 223, 1226–1229. <https://doi.org/10.1038/2231226a0>
1573
1574 955 Noffke, N., Eriksson, K.A., Hazen, R.M., Simpson, E.L., 2006. A new window into Early Archean life:
1575 956 Microbial mats in Earth’s oldest siliciclastic tidal deposits (3.2 Ga Moodies Group, South Africa).
1576 957 *Geology* 34, 253. <https://doi.org/10.1130/G22246.1>
1578 958 Nutman, A.P., Bennett, V.C., Friend, C.R.L., Van Kranendonk, M.J., Chivas, A.R., 2016. Rapid
1579 959 emergence of life shown by discovery of 3,700-million-year-old microbial structures. *Nature* 537,
1580 960 535–538. <https://doi.org/10.1038/nature19355>
1581 961
1582 961 Oehler, D.Z., Schopf, J.W., Kvenvolden, K.A., 1972. Carbon Isotopic Studies of Organic Matter in
1583 962 Precambrian Rocks. *Science* (80-.). 175, 1246–1248. <https://doi.org/10.1126/science.175.4027.1246>
1584 962
1585 963 Oehler, D.Z., Walsh, M.M., Sugitani, K., Liu, M.C., House, C.H., 2017. Large and robust lenticular
1586 964 microorganisms on the young Earth. *Precambrian Res.* 296, 112–119.
1587 964
1588 965 <https://doi.org/10.1016/j.precamres.2017.04.031>
1589 965
1590 966 Oehler, D.Z., Walter, M.R., Sugitani, K., Allwood, A., Meibom, A., Mostefaoui, S., Selo, M., Thomen,
1591 967 A., Gibson, E.K., 2009. NanoSIMS : Insights to biogenicity and syngeneity of Archaean
1592 968 carbonaceous structures 173, 70–78. <https://doi.org/10.1016/j.precamres.2009.01.001>
1593 968
1594 969 Otálora, F., Mazurier, A., Garcia-Ruiz, J.M., Van Kranendonk, M.J., Kotopoulou, E., El Albani, A.,
1595 970 Garrido, C.J., 2018. A crystallographic study of crystalline casts and pseudomorphs from the 3.5 Ga
1596 970 dresser formation, Pilbara Craton (Australia). *J. Appl. Crystallogr.* 51, 1050–1058.
1597 971
1598 972 <https://doi.org/10.1107/S1600576718007343>
1599 972
1600 973 Pflug, H.D., 1967. Structured organic remains from the Fig Tree Series (Precambrian) of the Barberton
1601 974 mountain land (South Africa). *Rev. Palaeobot. Palynol.* 5, 9–29. [https://doi.org/10.1016/0034-](https://doi.org/10.1016/0034-6667(67)90205-9)
1602 974
1603 975 [6667\(67\)90205-9](https://doi.org/10.1016/0034-6667(67)90205-9)
1604 975
1605 976 Pflug, H.D., 1966. Structured organic remains from the Fig Tree Series (Precambrian) of the Barberton
1606 977 Mountain land (South Africa). *Econ. Geol. Res. Unit, Univ. Witwatersrand, Johannesburg, Inform.*
1607 978 *Circ.* 28, 14.
1608 978
1609 979 Pflug, H.D., Meinel, W., Neumann, K.H., Meinel, M., 1969. Entwicklungstendenzen des frühen Lebens
1610 980 auf der Erde. *Naturwissenschaften* 56, 10–14. <https://doi.org/10.1007/BF00599585>
1611 980
1612 981 Rasmussen, B., Blake, T.S., Fletcher, I.R., Kilburn, M.R., 2009. Evidence for microbial life in
1613 982 synsedimentary cavities from 2.75 Ga terrestrial environments. *Geology* 37, 423–426.
1614 982
1615 983 <https://doi.org/10.1130/G25300A.1>
1616 983
1617 984 Schieber, J., Bose, P.K., Eriksson, P.G., 2007. Atlas of microbial mat features preserved within the
1618 985 siliciclastic rock record. Elsevier, Amsterdam.
1619 986
1620 986 Schopf, J.W., 2004. Geochemical and submicron-scale morphologic analyses of individual Precambrian
1621
1622
1623
1624

1625
1626
1627 987 microorganisms. *Geochemical Soc. Spec. Publ.* 365–375.
1628 988 Schopf, J.W., 1975. Precambrian Paleobiology: Problems and Perspectives. *Annu. Rev. Earth Planet. Sci.*
1629 989 3, 213–249. <https://doi.org/10.1146/annurev.ea.03.050175.001241>
1631 990 Schopf, J.W., Barghoorn, E.S., 1967. Alga-Like Fossils from the Early Precambrian of South Africa.
1632 991 *Science* (80-.). 156, 508–512. <https://doi.org/10.1126/science.156.3774.508>
1634 992 Schopf, J.W., Walter, M.R., 1983. Archean microfossils: new evidence of ancient microbes, in: Schopf,
1635 993 J.W. (Ed.), *Earth's Earliest Biosphere: Its Origin and Evolution*. Princeton University Press,
1636 994 Princeton, pp. 214–239.
1638 995 Simpson, E.L., Eriksson, K.A., Mueller, W.U., 2012. 3.2 Ga eolian deposits from the Moodies Group,
1639 996 Barberton Greenstone Belt, South Africa: Implications for the origin of first-cycle quartz
1641 997 sandstones. *Precambrian Res.* 214–215, 185–191. <https://doi.org/10.1016/j.precamres.2012.01.019>
1643 998 Sleep, N.H., Zahnle, K.J., Kasting, J.F., Morowitz, H.J., 1989. Annihilation of ecosystems by large
1644 999 asteroid impacts on the early Earth. *Nature* 342, 139–142. <https://doi.org/10.1038/342139a0>
1646 1000 Staudigel, H., Furnes, H., Dewit, M., 2015. Paleoarchean trace fossils in altered volcanic glass 112.
1647 1001 <https://doi.org/10.1073/pnas.1421052112>
1648 1002 Stüeken, E.E., Kipp, M.A., Koehler, M.C., Buick, R., 2016. The evolution of Earth's biogeochemical
1650 1003 nitrogen cycle. *Earth-Science Rev.* 160, 220–239. <https://doi.org/10.1016/j.earscirev.2016.07.007>
1651 1004 Sugitani, K., Grey, K., Allwood, A., Nagaoka, T., Mimura, K., Minami, M., Marshall, C.P., Van
1653 1005 Kranendonk, M.J., Walter, M.R., 2007. Diverse microstructures from Archaean chert from the
1654 1006 Mount Goldsworthy-Mount Grant area, Pilbara Craton, Western Australia: Microfossils,
1655 1007 dubiofossils, or pseudofossils? *Precambrian Res.* 158, 228–262.
1657 1008 <https://doi.org/10.1016/j.precamres.2007.03.006>
1659 1009 Sugitani, K., Lepot, K., Nagaoka, T., Mimura, K., Van Kranendonk, M., Oehler, D.Z., Walter, M.R.,
1660 1010 2010. Biogenicity of Morphologically Diverse Carbonaceous Microstructures from the *ca.* 3400 Ma
1661 1011 Strelley Pool Formation, in the Pilbara Craton, Western Australia. *Astrobiology* 10, 899–920.
1663 1012 <https://doi.org/10.1089/ast.2010.0513>
1664 1013 Sugitani, K., Mimura, K., Nagaoka, T., Lepot, K., Takeuchi, M., 2013. Microfossil assemblage from the
1666 1014 3400Ma Strelley Pool Formation in the Pilbara Craton, Western Australia: Results from a new
1667 1015 locality. *Precambrian Res.* 226, 59–74. <https://doi.org/10.1016/j.precamres.2012.11.005>
1669 1016 Taj, R.J., Aref, M. a. M., Schreiber, B.C., 2014. The influence of microbial mats on the formation of sand
1670 1017 volcanoes and mounds in the Red Sea coastal plain, south Jeddah, Saudi Arabia. *Sediment. Geol.*
1672 1018 311, 60–74. <https://doi.org/10.1016/j.sedgeo.2014.06.006>
1673 1019 Tice, M.M., 2009. Environmental Controls on Photosynthetic Microbial Mat Distribution and
1674 1020 Morphogenesis on a 3.42Ga Clastic-Starved Platform. *Astrobiology* 9, 989–1000.
1676
1677
1678
1679
1680

1681
1682
1683 1021 Tice, M.M., Bostick, B.C., Lowe, D.R., 2004. Thermal history of the 3.5-3.2 Ga Onverwacht and Fig
1684 1022 Tree Groups, Barberton greenstone belt, South Africa, inferred by Raman microspectroscopy of
1685 1023 carbonaceous material. *Geology* 32, 37–40. <https://doi.org/10.1130/G19915.1>
1687 1024 Tice, M.M., Lowe, D.R., 2006a. The origin of carbonaceous matter in pre-3.0 Ga greenstone terrains: A
1688 1025 review and new evidence from the 3.42 Ga Buck Reef Chert. *Earth-Science Rev.* 76, 259–300.
1690 1026 <https://doi.org/10.1016/j.earscirev.2006.03.003>
1691 1027 Tice, M.M., Lowe, D.R., 2006b. Hydrogen-based carbon fixation in the earliest known photosynthetic
1692 1028 organisms. *Geology* 34, 37. <https://doi.org/10.1130/G22012.1>
1694 1029 Tice, M.M., Lowe, D.R., 2004. Photosynthetic microbial mats in the 3, 416-Myr-old ocean. *Nature* 431,
1695 1030 549–552. <https://doi.org/10.1038/nature02920.1>.
1697 1031 Tice, M.M., Thornton, D.C.O., Pope, M.C., Olszewski, T.D., Gong, J., 2011. Archean Microbial Mat
1698 1032 Communities. *Annu. Rev. Earth Planet. Sci.* 39, 297–319. [https://doi.org/10.1146/annurev-earth-](https://doi.org/10.1146/annurev-earth-040809-152356)
1700 1033 [040809-152356](https://doi.org/10.1146/annurev-earth-040809-152356)
1702 1034 Toulkeridis, T., Goldstein, S.L., Clauer, N., Kröner, A., Todt, W., Schidlowski, M., 1998. Sm-Nd, Rb-Sr
1703 1035 and Pb-Pb dating of silicic carbonates from the early Archaean Barberton Greenstone Belt, South
1704 1036 Africa: evidence for post-depositional isotopic resetting at low temperature. *Precambrian Res.* 92,
1706 1037 129–144.
1707 1038 Trower, E.J., Lowe, D.R., 2016. Sedimentology of the ~3.3Ga upper Mendon Formation, Barberton
1709 1039 Greenstone Belt, South Africa. *Precambrian Res.* 281, 473–494.
1710 1040 <https://doi.org/10.1016/j.precamres.2016.06.003>
1712 1041 Van Kranendonk, M.J., Philippot, P., Lepot, K., Bodorkos, S., Pirajno, F., 2008. Geological setting of
1713 1042 Earth's oldest fossils in the ca. 3.5 Ga Dresser Formation, Pilbara Craton, Western Australia.
1714 1043 *Precambrian Res.* 167, 93–124. <https://doi.org/10.1016/j.precamres.2008.07.003>
1716 1044 van Zuilen, M.A., Chaussidon, M., Rollion-Bard, C., Marty, B., 2007. Carbonaceous cherts of the
1717 1045 Barberton Greenstone Belt, South Africa: Isotopic, chemical and structural characteristics of
1719 1046 individual microstructures. *Geochim. Cosmochim. Acta* 71, 655–669.
1720 1047 <https://doi.org/10.1016/j.gca.2006.09.029>
1722 1048 Viljoen, M.J., Viljoen, R.P., 1969. An introduction to the geology of the Barberton granite-greenstone
1723 1049 terrain. *Spec. Publ. Geol. Soc. S. Afr* 2, 9–28.
1725 1050 Visser, D., 1956. The geology of the Barberton area. *Geol. Soc. S. Afr. Spec. Publ.* 15, 253.
1726 1051 Wacey, D., 2012. Earliest evidence for life on Earth: An Australian perspective. *Aust. J. Earth Sci.* 59,
1727 1052 153–166. <https://doi.org/10.1080/08120099.2011.592989>
1729 1053 Wacey, D., 2009. Early Life on Earth. A Practical Guide, Topics in Geobiology, Vol. 31. Springer.
1730 1054 Wacey, D., Fisk, M., Saunders, M., Eiloart, K., Kong, C., 2017. Critical testing of potential cellular
1731 1732
1733
1734
1735
1736

1737
1738
1739 1055 structures within microtubes in 145 Ma volcanic glass from the Argo Abyssal Plain. *Chem. Geol.*
1740 1056 466, 575–587. <https://doi.org/10.1016/j.chemgeo.2017.07.006>
1741
1742 1057 Wacey, D., Noffke, N., Saunders, M., Guagliardo, P., Pyle, D.M., 2018a. Volcanogenic Pseudo-Fossils
1743 1058 from the ~3.48 Ga Dresser Formation, Pilbara, Western Australia. *Astrobiology* 18, ast.2017.1734.
1744
1745 1059 <https://doi.org/10.1089/ast.2017.1734>
1746 1060 Wacey, D., Saunders, M., Kong, C., 2018b. Remarkably preserved tephra from the 3430 Ma Strelley Pool
1747
1748 1061 Formation, Western Australia: Implications for the interpretation of Precambrian microfossils. *Earth*
1749 1062 *Planet. Sci. Lett.* 487, 33–43. <https://doi.org/10.1016/j.epsl.2018.01.021>
1750
1751 1063 Walsh, M.M., 2004. Evaluation of Early Archean Volcaniclastic and Volcanic Flow Rocks as Possible
1752 1064 Sites for Carbonaceous Fossil Microbes. *Astrobiology* 4, 429–437.
1753
1754 1065 <https://doi.org/10.1089/ast.2004.4.429>
1755 1066 Walsh, M.M., 1992. Microfossils and possible microfossils from the Early Archean Onverwacht Group,
1756 1067 Barberton Mountain Land, South Africa. *Precambrian Res.* 54, 271–293.
1757
1758 1068 Walsh, M.M., Lowe, D.R., 1999. Modes of accumulation of carbonaceous matter in the Early Archean: a
1759 1069 petrographic and geochemical study of the carbonaceous cherts of the Swaziland Supergroup, in:
1760
1761 1070 Lowe, D.R., Byerly, G.R. (Eds.), *Geologic Evolution of the Barberton Greenstone Belt, South*
1762 1071 *Africa. Geological Society of America Special Paper* 329, pp. 115–132.
1763
1764 1072 Walsh, M.M., Lowe, D.R., 1985. Filamentous microfossils from the 3,500-Myr-old Onverwacht Group,
1765 1073 Barberton Mountain Land, South Africa. *Nature* 314, 530–531.
1766
1767 1074 Walter, M.R., Buick, R., Dunlop, J.S.R., 1980. Stromatolites 3,400-3,500 Myr old from the North Pole
1768 1075 area, Western Australia. *Nature*. <https://doi.org/10.1038/284443a0>
1769
1770 1076 Westall, F., Campbell, K.A., Bréhéret, J.G., Foucher, F., Gautret, P., Hubert, A., Sorieul, S., Grassineau,
1771 1077 N., Guido, D.M., 2015. Archean (3.33 Ga) microbe-sediment systems were diverse and flourished in
1772 1078 a hydrothermal context. *Geology* 43, 615–618. <https://doi.org/10.1130/G36646.1>
1773
1774 1079 Westall, F., Cavalazzi, B., Lemelle, L., Marrocchi, Y., Rouzard, J.N., Simionovici, A., Salomé, M.,
1775 1080 Mostefaoui, S., Andreazza, C., Foucher, F., Toporski, J., Jauss, A., Thiel, V., Southam, G.,
1776
1777 1081 MacLean, L., Wirick, S., Hofmann, A., Meibom, A., Robert, F., Défarge, C., 2011. Implications of
1778 1082 in situ calcification for photosynthesis in a ~3.3Ga-old microbial biofilm from the Barberton
1779
1780 1083 greenstone belt, South Africa. *Earth Planet. Sci. Lett.* 310, 468–479.
1781 1084 <https://doi.org/10.1016/j.epsl.2011.08.029>
1782
1783 1085 Westall, F., de Ronde, C.E., Southam, G., Grassineau, N., Colas, M., Cockell, C., Lammer, H., 2006.
1784 1086 Implications of a 3.472-3.333 Gyr-old subaerial microbial mat from the Barberton greenstone belt,
1785
1786 1087 South Africa for the UV environmental conditions on the early Earth. *Philos. Trans. R. Soc. B Biol.*
1787 1088 *Sci.* 361, 1857–1876. <https://doi.org/10.1098/rstb.2006.1896>
1788
1789
1790
1791
1792

1793
1794
1795 1089 Westall, F., De Wit, M.J., Dann, J., Van der Gaast, S., De Ronde, C.E.J., Gerneke, D., 2001. Early
1796 1090 archeon fossil bacteria and biofilms in hydrothermally-influenced sediments from the Barberton
1797 greenstone belt, South Africa. *Precambrian Res.* 106, 93–116. <https://doi.org/10.1016/S0301->
1798 1091
1799 1092 9268(00)00127-3
1800
1801 1093 Westall, F., Hickman-Lewis, K., Hinman, N., Gautret, P., Campbell, K.A., Bréhéret, J.G., Foucher, F.,
1802 1094 Hubert, A., Sorieul, S., Dass, A.V., Kee, T.P., Georgelin, T., Brack, A., 2018. A Hydrothermal-
1803 1095 Sedimentary Context for the Origin of Life. *Astrobiology* 18, 259–293.
1804
1805 1096 <https://doi.org/10.1089/ast.2017.1680>
1806 1097 Williford, K.H., Ushikubo, T., Lepot, K., Kitajima, K., Hallmann, C., Spicuzza, M.J., Kozdon, R.,
1807 1098 Eigenbrode, J.L., Summons, R.E., Valley, J.W., 2016. Carbon and sulfur isotopic signatures of
1808 1099 ancient life and environment at the microbial scale: Neoproterozoic shales and carbonates. *Geobiology*
1809 1100 14, 105–128. <https://doi.org/10.1111/gbi.12163>
1810
1811 1101 Williford, K.H., Ushikubo, T., Schopf, J.W., Lepot, K., Kitajima, K., Valley, J.W., 2013. Preservation
1812 1102 and detection of microstructural and taxonomic correlations in the carbon isotopic compositions of
1813 1103 individual Precambrian microfossils. *Geochim. Cosmochim. Acta* 104, 165–182.
1814
1815 1104 <https://doi.org/10.1016/j.gca.2012.11.005>
1816
1817 1105 Xie, X., Byerly, G.R., Ferrell Jr., R.E., 1997. IIB trioctahedral chlorite from the Barberton greenstone belt:
1818 1106 crystal structure and rock composition constraints with implications to geothermometry. *Contrib. to*
1819 1107 *Mineral. Petrol.* 126, 275–291. <https://doi.org/10.1007/s004100050250>
1820
1821 1108
1822
1823
1824
1825
1826
1827
1828
1829
1830
1831
1832
1833
1834
1835
1836
1837
1838
1839
1840
1841
1842
1843
1844
1845
1846
1847
1848

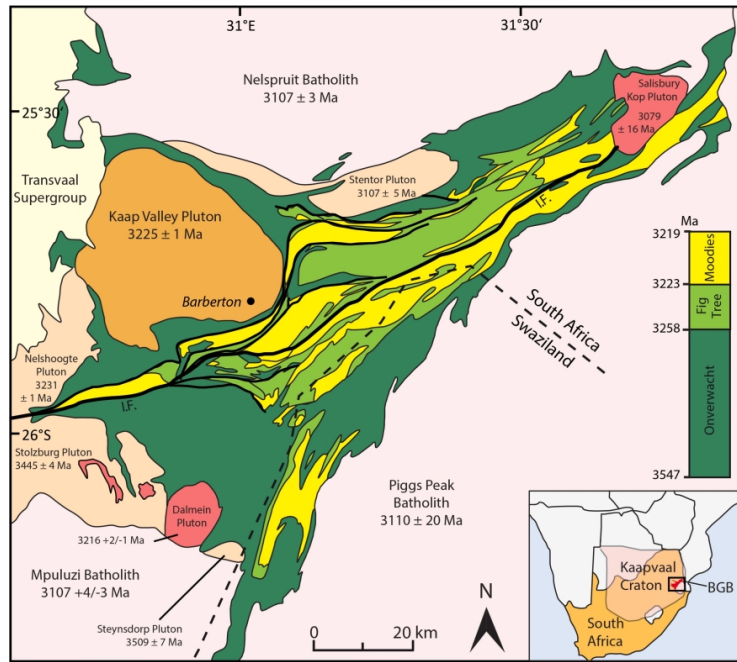


Fig. 1. Geological map of the Barberton Greenstone Belt (BGB) of South Africa and Swaziland and its surrounding plutons in the eastern part of the Kaapvaal Craton. The Barberton Supergroup comprises from base to top the Onverwacht, Fig Tree, and Moodies Group.

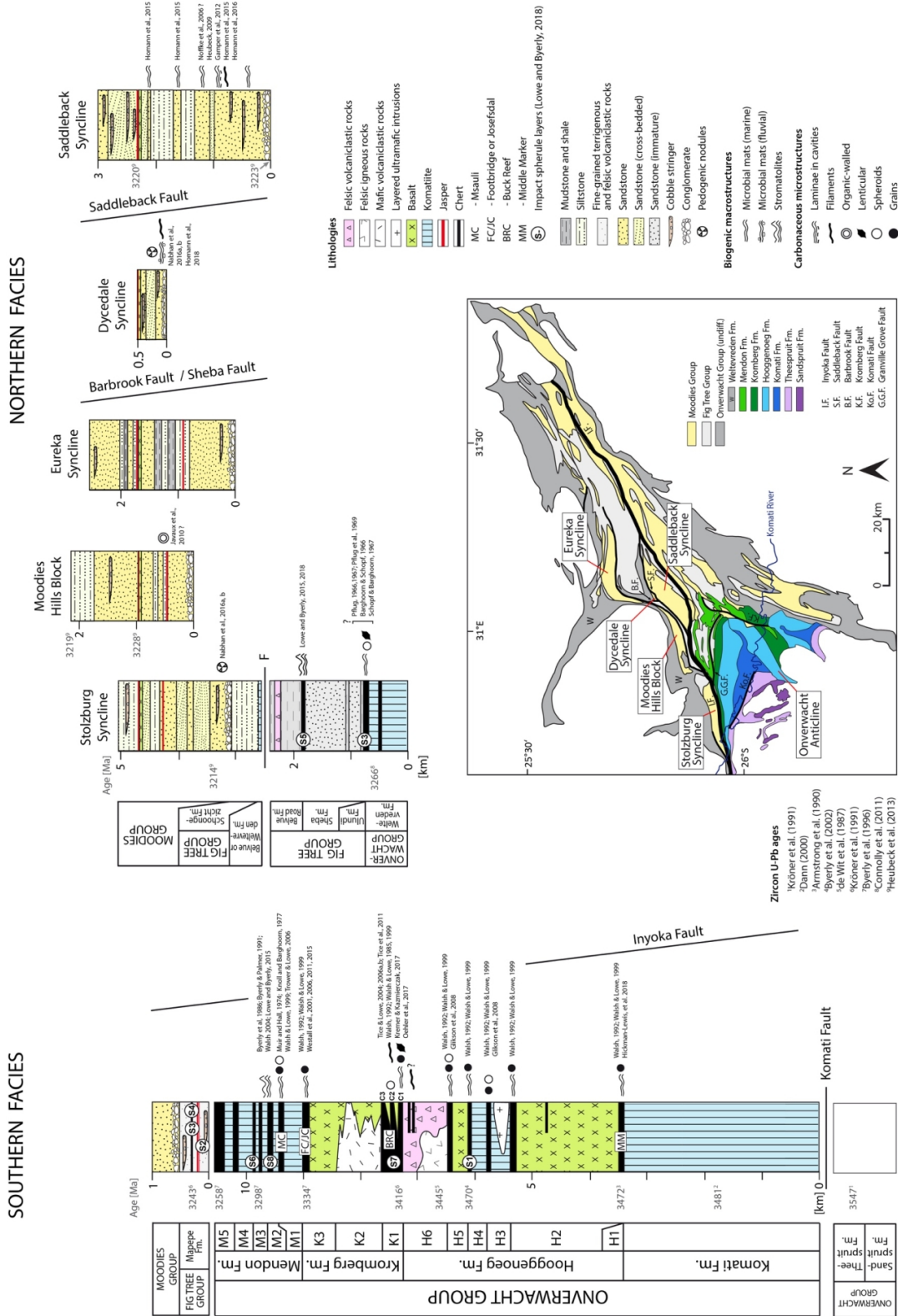


Fig. 2. Generalized stratigraphy and structure of the Barberton Supergroup north and south of the Inyoka Fault (mod. after Lowe and Byerly, 1999) with indicated stratigraphic position of reported macro- and microscopic traces of Paleoproterozoic life in the Barberton Greenstone Belt.

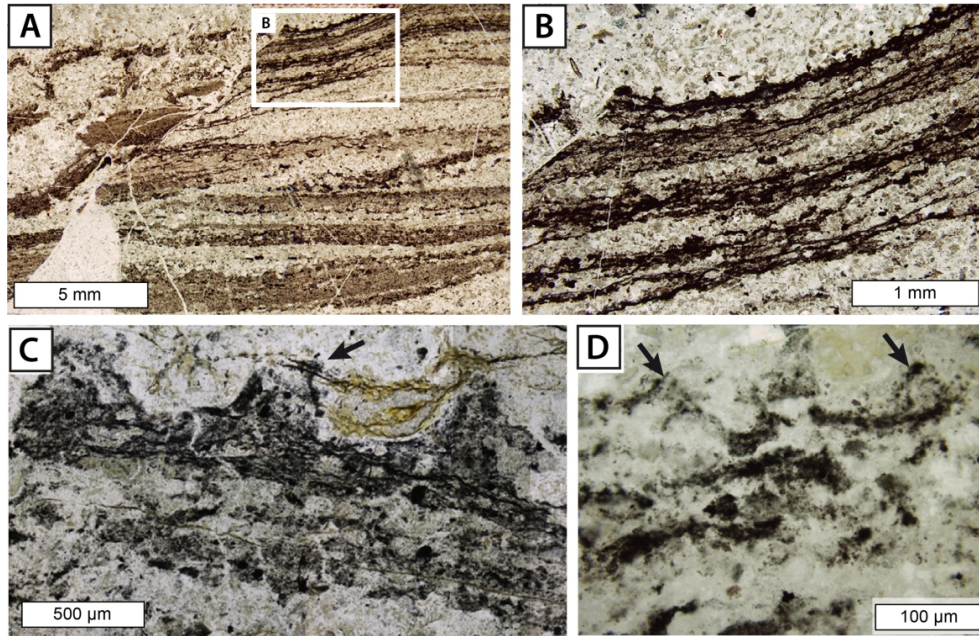


Fig. 3. Photomicrographs of carbonaceous laminations from silicified volcaniclastic sediments of the 3.47 Ga Middle Marker interpreted as remnants of microbial mats. A) Multi-layered mats on horizontally-laminated and cross-bedded sediments, disrupted by secondary fracture. B) Close-up view of crinkly, 'micro-tufted' laminations. C and D) Laminations with secondary 'pseudo-tufted' morphology (arrows), which likely formed due to plastic deformation. *Images (A-D) from Hickman-Lewis et al. (2018).*

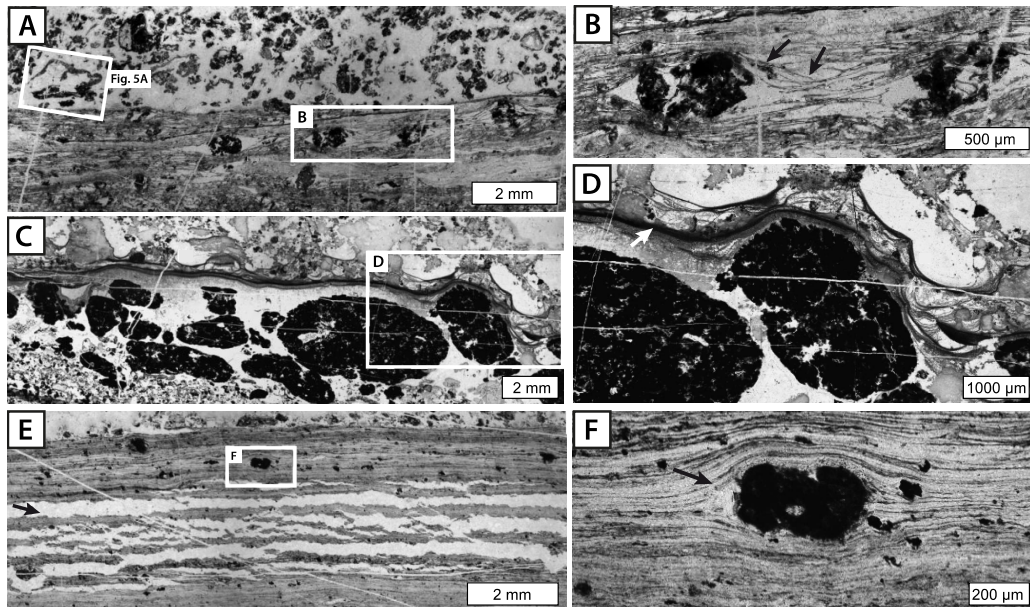


Fig. 4. Photomicrographs of morphologically diverse types of carbonaceous laminations preserved in the 3.42 Ga Buck Reef Chert and interpreted as fossil microbial mats. A and B) Alpha-type laminations loosely draping trapped grains (arrows) and overlain by detrital sediment layer with eroded mat fragment. C and D) Beta-type laminations with fine meshworks of filament-like strands that drape underlying detrital carbonaceous and silica grains (arrow). E) Gamma-type laminations dissected by early diagenetic silica veins subparallel to bedding (arrow), likely formed due to fluid escape from the sediment. F) Close-up view showing flat carbonaceous laminations, which tightly drape a detrital grain (arrow). *Images (A-F) from Tice (2009).*

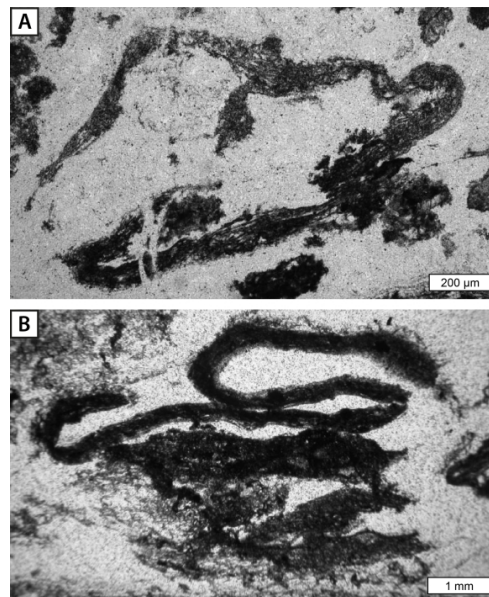


Fig. 5. Photomicrographs of eroded and rolled-up microbial mat fragments from the Buck Reef Chert. A) Close-up view of boxed area in Fig. 4A showing a plastically-deformed segment of alpha-type mat. B) Large, rolled-up fragment of a beta-type mat. *Image (A) from Tice (2009) and (B) from Tice and Lowe 2006b.*

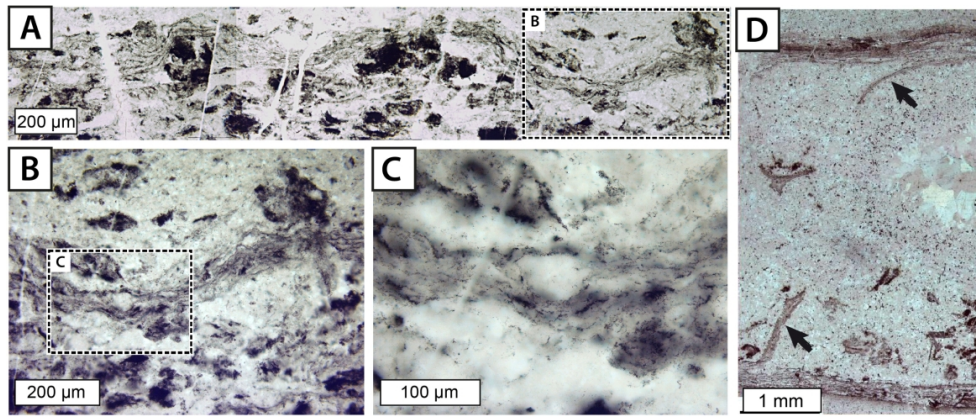


Fig. 6. Photomicrographs of microbial biofilms preserved in the 3.33 Ga Josefsdal Chert. A) Wispy anastomosing laminations that coat and stabilize the underlying sediments. B and C) Close-up views of the fine carbonaceous layers. D) Partially eroded fragments facing down and upwards (arrows) indicate pliable consistency of the biofilms. *Images (A-C) from Westall et al. (2011); Image (D) from Westall et al. (2015).*

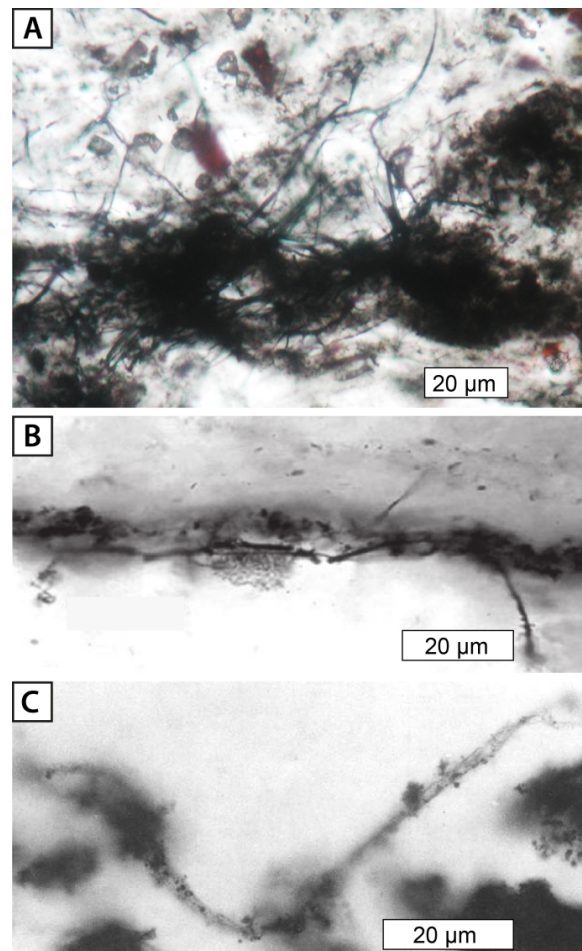


Fig. 7. Photomicrographs of filamentous microstructures from the Buck Reef Chert (Kromberg Formation). A) Interwoven clumps of filamentous microfossils. B) Hollow cylindrical filaments oriented subparallel to bedding. C) Solitary, slightly twisted hollow filament. *Image (A) courtesy of Maud M. Walsh; Image (B) from Walsh (2000); Image (C) from Walsh (1992).*

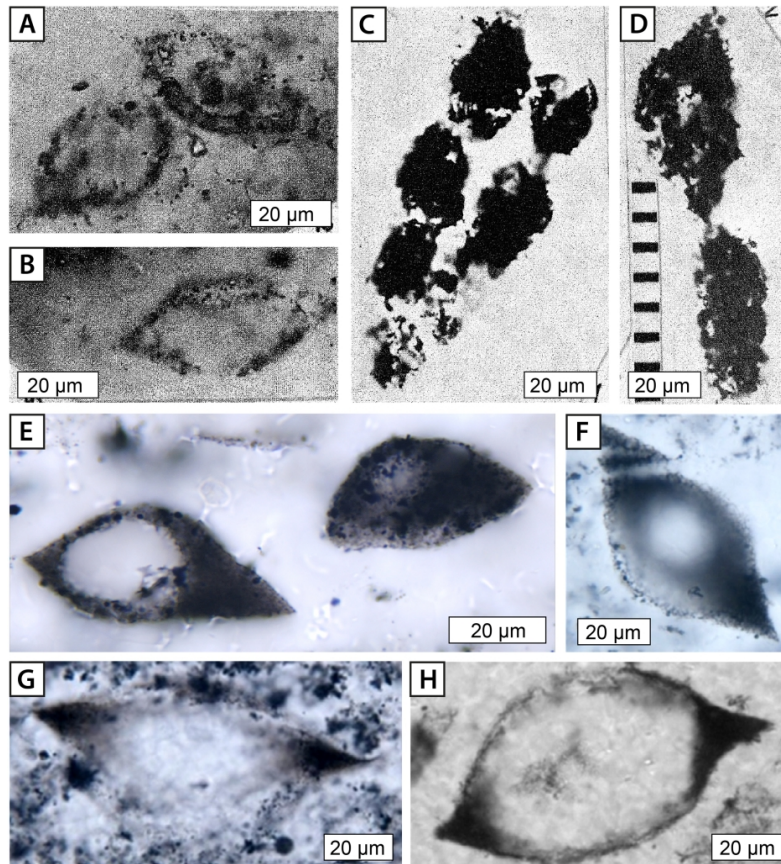


Fig. 8. Photomicrographs of lenticular structures interpreted as microfossils. A-D) Lenticular, disk-shaped objects with hollow centers and carbonaceous walls preserved in cherts from the Upper Onverwacht Group. Note that the structures occur isolated or in chain-like clusters of several specimen. (E-H) Morphologically very similar lenticular microfossils from the Buck Reef Chert. *Images (A-D) from Pflug (1966); Images (E-H) from Oehler et al. (2017), courtesy of Dorothy Z. Oehler.*

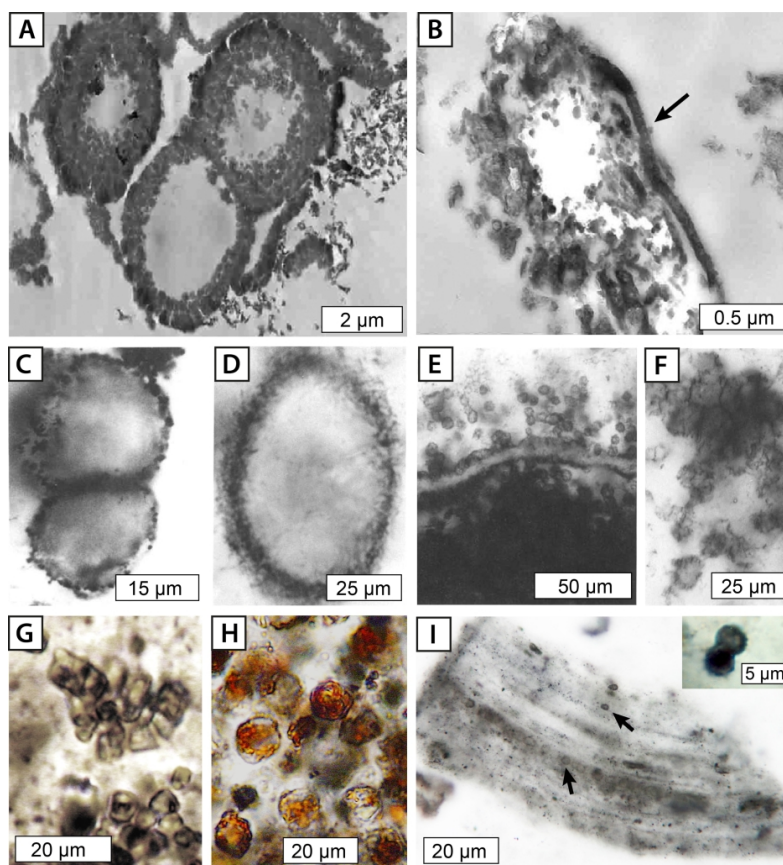


Fig. 9. Photomicrographs of proposed spheroidal microfossils from cherts of the Onverwacht Group. A and B) Transmission electron microscopy (TEM) images of cell-like objects with granular, in places detached walls (arrow) from the Hooggenoeg Formation. C and D) Large spheroids and ellipsoids from the Buck Reef Chert. E and F) Clusters of thin-walled spheroids from the Buck Reef Chert. G and H) Groups of spheroidal microstructures with rounded to angular walls from the Buck Reef Chert. I) Putative organic microspheres (arrows) from the Msauli Chert, which show features resembling cell division (small image in the upper right corner). Images (A-D) from Glikson *et al.* (2008); Images (C-F) from Walsh (1992); Images (G and H) from Kremer and Kazmierczak (2017); Image (I) courtesy of Andrew H. Knoll.

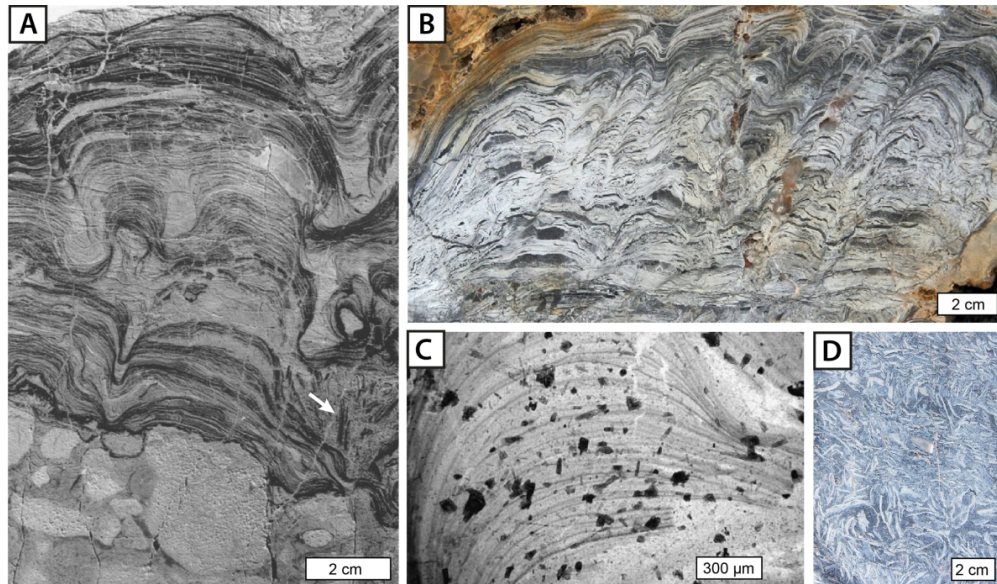


Fig. 10. Putative stromatolites and laminated silica crusts from the upper Onverwacht and Fig Tree Group. A) Polished slab showing morphologically diverse stromatolites overlying and draping the brecciated top of a komatiitic lava flow. Small basal domes successively grade into pseudocolumnar stromatolites with bridging laminations that are, in turn, overlain by low-relief domal laminations. Note the eroded stromatolite chips adjacent to the basal dome (arrow). B) Laminated silica crusts with inclined stromatolite-like columns and domes. C) Photomicrograph showing fine primary carbonaceous laminae with variable enrichment in secondary fine-grained tourmaline (dark minerals). D) Conglomerate of laminated silica chips interpreted as fragments of eroded stromatolites or sinter crusts. *Images (A and C) from Byerly and Palmer (1991), (B and D) from Lowe and Byerly (2018).*

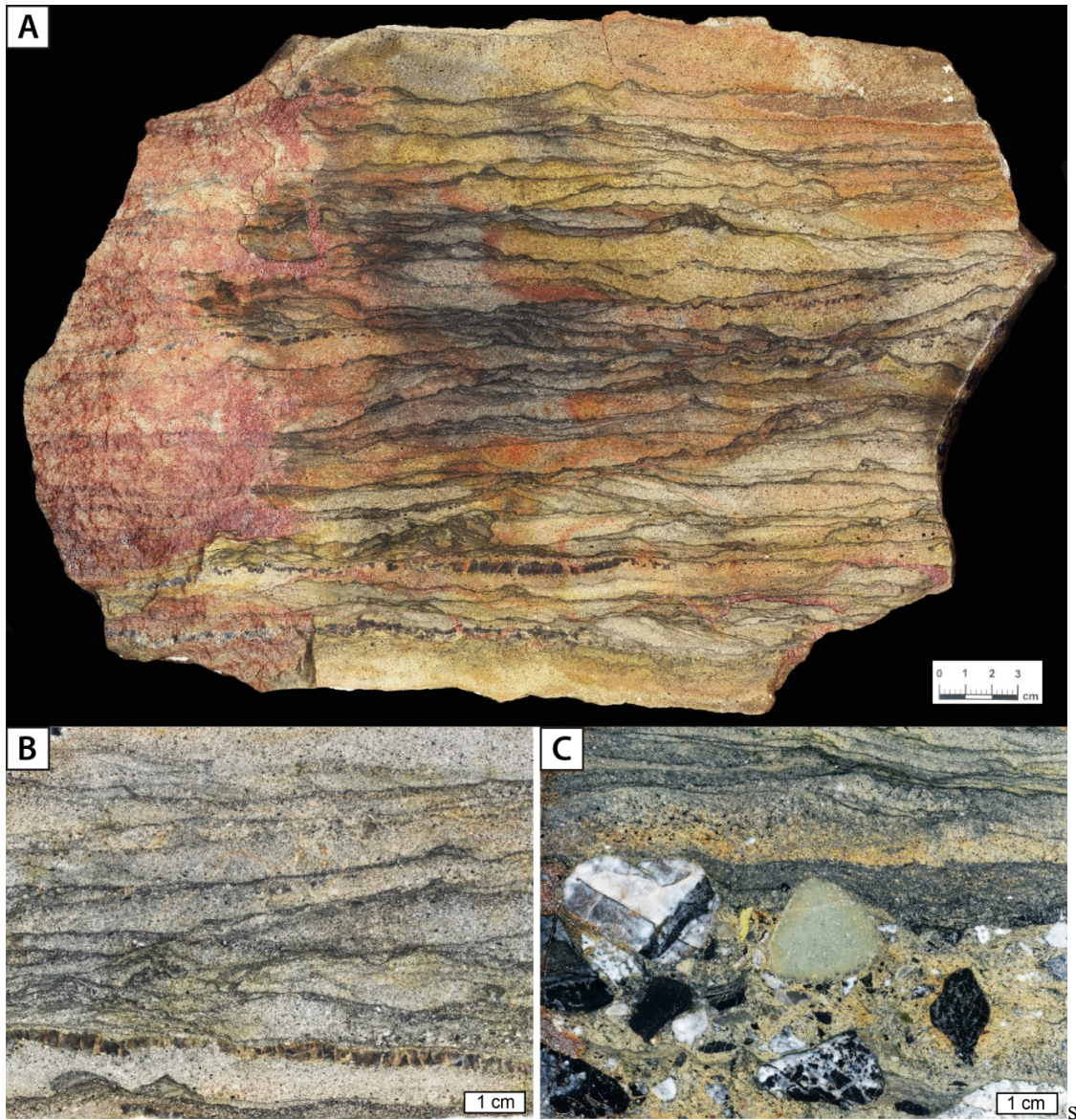


Fig. 11. Comparison of fossil microbial mats from tidal marine (A, B) and fluvial (C) deposits of the 3.22 Ga Moodies Group. A, B) Polished slab photographs of marine mats from the Saddleback Syncline showing densely spaced, crinkly carbonaceous laminations with small domes and tufts. The fossil mats are interbedded with medium- to coarse-grained sandstone and in places underlain by bedding-parallel chert lenses interpreted as silicified cavities. C) Terrestrial mats from the fluvial deposits of the Dycedale Syncline draping and onlapping interbedded clasts. Note that the preserved carbonaceous laminae are often thicker in comparison with the marine mats.

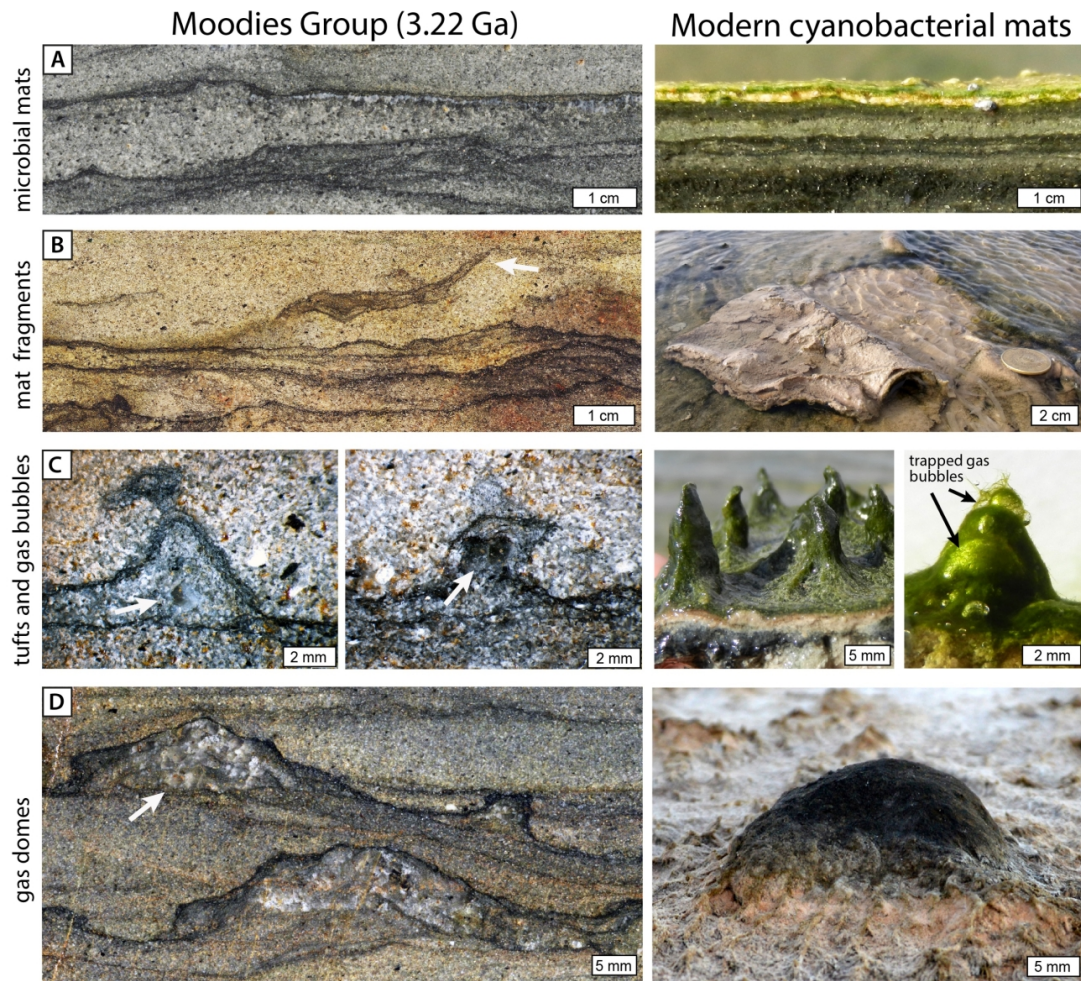


Fig. 12. Comparison of fossil intertidal microbial mats from the 3.22 Ga Moodies Group (left) with modern cyanobacterial mats from the tidal flats of Bahar Alouane, Tunisia (right). A) Crinkly carbonaceous mat laminations. B) Eroded mat fragment (arrow) and roll-up structure indicative for a cohesive consistency. C) Microbial tufts with now silicified cavities (arrows) interpreted as fossil gas bubbles, resembling trapped oxygen-rich bubbles in modern tufted mats. D) Silicified gas domes beneath the Moodies mats (arrow) and modern analogue of similar shape and size from Tunisia.

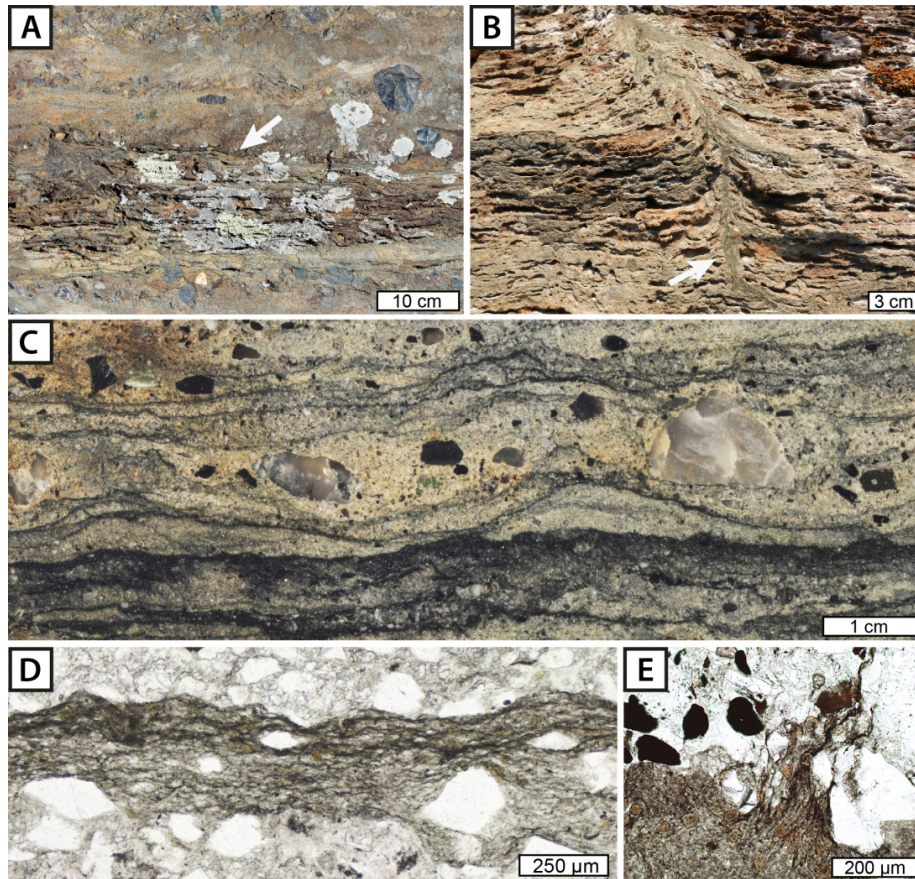


Fig. 13. Fossil terrestrial microbial mats from fluvial sandstones and conglomerates of the Moodies Group. A) Field photograph of the fluvial mats (arrow) interbedded with gravelly sandstones. B) Microbial mats disrupted and deformed by subvertical fluid-escape structure with well-defined central channel (arrow). C) Polished slab photograph with dark carbonaceous laminae of the fossil mats, draping former sedimentary surfaces and overlapping pebbles. D) Close-up view of the laminae, which show a dense meshwork of interwoven filamentous microstructures with trapped detrital grains. E) Filament-like microstructures in the upper, partially eroded part of the mat. *Images (A-E) from Homann et al. (2018).*

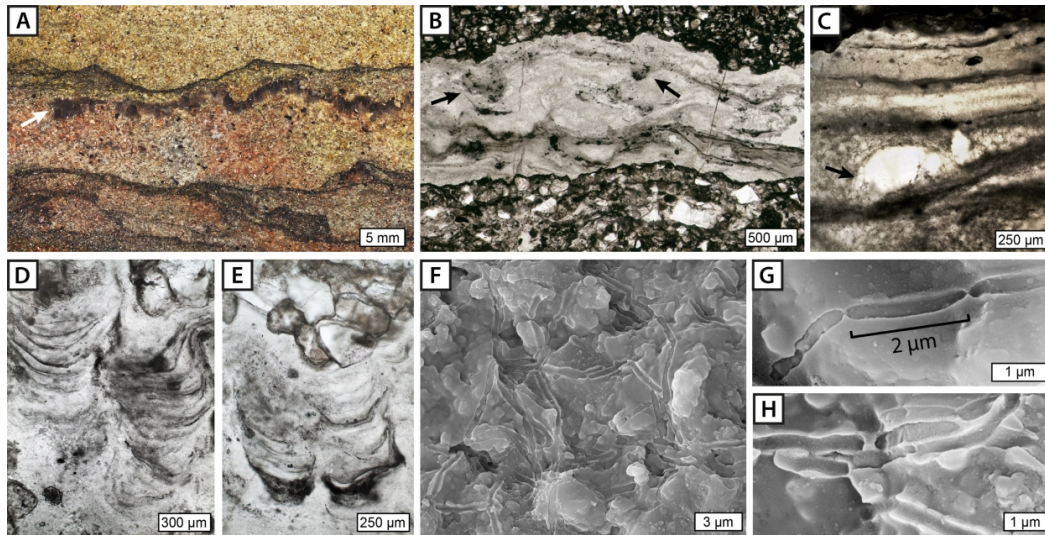


Fig. 14. Evidence for cavity-dwelling microbial life in the tidal deposits of the Moodies Group. A) Polished slab photograph showing silicified bedding-parallel cavity beneath fossil microbial mat (arrow). B) Photomicrograph of the silicified cavities with carbonaceous laminations, wisps, and pendant protrusions at the cavity ceiling (arrows). C) Carbonaceous laminae surrounding ovoid-shaped structure interpreted as trapped gas bubble (arrow). D and E) Close-up view of downward-facing columnar microstromatolites with preserved internal carbonaceous laminae. F) SEM image showing meshwork of filament molds embedded and permineralized in chert. G and H) Filamentous molds with regularly spaced, rod-shaped segments of approximately similar length. *Images (B and D-H) from Homann et al. (2016).*

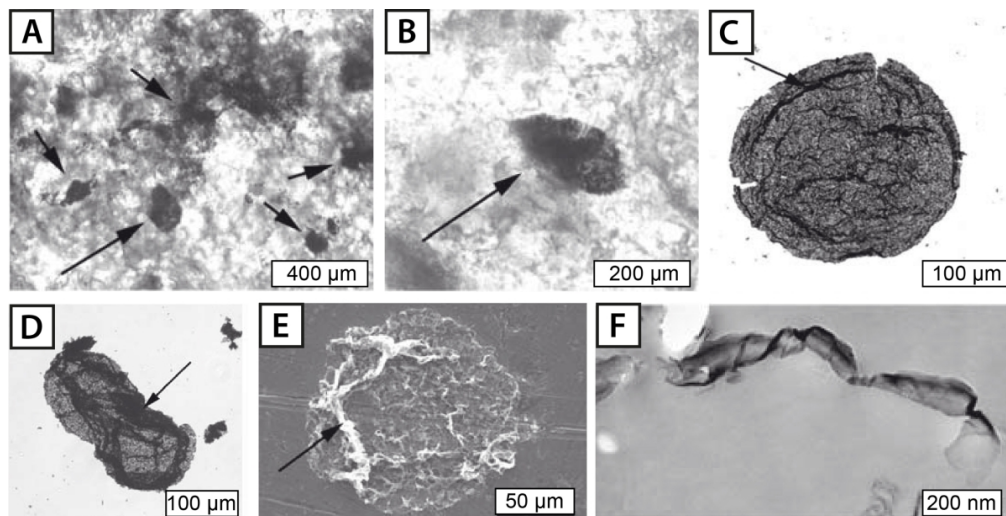


Fig. 15. Large organic-walled microfossils from the Moodies Group. A and B) Compressed spheroidal structures (arrows) in petrographic thin section. C and D) Microstructure extracted from the rock by acid maceration showing concentric folding (arrow in C) and collapse (arrow in D) of the wall. E) SEM image showing the folded, wrinkled and degraded texture of the wall (arrow). F) TEM image of ultrathin section showing homogenous ultrastructure of the torn and wrinkled 'cell' wall. *Images (A-F) from Javaux et al. (2010).*

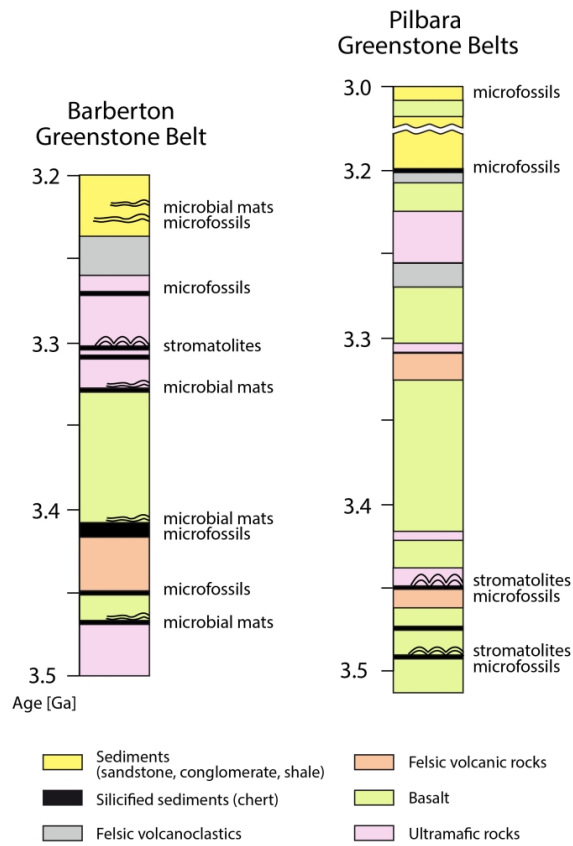


Fig. 15. Simplified stratigraphy and traces of early life in the Barberton Supergroup of South Africa in comparison with the Pilbara Supergroup of Western Australia.

Table 1 | Claims for Paleoproterozoic Life in the Barberton Greenstone Belt, South Africa

Age [Ma]	Lithostratigraphic Unit	Paleoenvironment	Morphological Evidence	Geochemical Evidence	Comments
~3220†	Mooides Group	Tidal marine coastline	Microbial mats: densely-spaced carbonaceous laminae interbedded with tidal sandstones (Nothke et al., 2006; Heubeck 2009; Gampert et al., 2012), cohesive erosion-resistant behavior, distinct mat morphologies (planar, crinkly, tufted); fossil gas bubbles, shrinkage cracks, eroded and reworked mat fragments, mm- to cm-sized silicified gas domes, and widespread fluid-escape structures (Homann et al., 2015).	$Bulk \delta^{13}C_{org}$: -33.9‰ to -21.3‰ (n=30) $Bulk \delta^{15}N$: -0.7‰ to +3.1‰ (n=9) Raman T_{max} : ~366°C	Well-established depositional, and petrographic context, widespread occurrence (15 km along strike), facies depended mat morphology, combined with evidence for biogeochemical cycling of carbon and nitrogen strongly suggest a biogenic origin (Homann et al., 2018).
~3250	Fig Tree Group Sheba Fm.	Shallow-marine deltaic?	Organic-walled microfossils: of carbonaceous composition preserved in shales and siltstones, spheroidal shape (up to 300 µm in diameter), cellular morphology and ultrastructure, occurrence in populations (Javaux et al., 2010; Butck, 2010).	$Bulk \delta^{13}C_{org}$: -28.3‰ to -16.4‰ (n=22)	A promising sign for life, carbon isotopes would be more convincing if measured in situ on individual microfossils.
		Braided fluvial to supratidal	Paleosols: containing pedogenic carbonates, sulfates, and pyrite grains with biogenic overgrowth rims (Nabhan et al., 2016a, b).	$In situ \delta^{34}S_{C-DTE}$: -25‰ and -20‰ (n=105) suggestive for microbial fractionation of sulfur	Detailed stratigraphic and petrographic context support Earth's oldest known signs for biogenic sulfur cycling on land.
		Fluvial, coastal braidedplain	Microbial mats: of carbonaceous composition (Homann et al., 2018), draping gravely sandstone beds and conglomerates of fluvial-alluvial origin (Heubeck and Lowe, 1994; Eriksson et al., 2006; Heubeck et al., 2016) associated with desiccation cracks, eroded mat fragments and fluid-escape structures.	$Bulk \delta^{13}C_{org}$: -23.6‰ to -17.9‰ (n=36) $Bulk \delta^{15}N$: +1.9‰ to +5.6‰ (n=10) Raman T_{max} : ~363°C	Earth's earliest combined fossil and geochemical evidence for the microbial colonization of terrestrial habitats on the emergent continental landmass.
3298±	Onverwacht Group Mendon Fm. (M2c)	Shallow-water to subaerial, evaporitic	Stromatolites: with tourmaline-rich, carbonaceous laminae preserved in cherts as laterally linked, low-relief domes (1–3 cm wide, 0.5–3 cm high) and compound domes or pseudocolumns of up to 10 cm height (Byerly et al., 1986; Byerly and Palmer, 1991). Fragments of eroded stromatolites or sinter crusts (Lowe and Byerly 2015, 2018).	None, except carbonaceous composition	Widespread (<10 km along strike) and morphological diverse. Possibly Africa's oldest stromatolites, but more evidence needed.
	Mendon Fm.* (previously named Swartkoppie Fm.)	?	Possible microfossils: lenticular [spindle-shaped] (30–70 µm in long axis) and spheroidal (5–50µm) shapes preserved in chert, occurrence as individuals or in clusters and chains, which might resemble remains of former colonies (Pflug 1966, 1967; Pflug et al., 1969). *Cherts were originally assigned to the Fig Tree Group.	None, except carbonaceous microfossil walls	Possible life, but geological context and geochemistry needed to further support biogenic origin.
	Mendon Fm.*	?	Possible microfossils: spheroidal structures, ~19 µm in diameter (Barghoorn and Schopf, 1966; Schopf and Barghoorn, 1967).	None, except carbonaceous microfossil walls	Simple morphology, and no depositional context or geochemistry reported. Could likely be non-biological (Wacey, 2009).
	Mendon Fm. (M1c) (Msauti Chert)	Shallow-marine to nearshore	Possible microfossils: spheroidal structures (1–4 µm in diameter) showing possible cell division (Knoll and Barghoorn, 1977).	None, except carbonaceous microfossil walls	Possible life, but hydrothermal fluids can mobilize and redistribute organic matter into spheroids (Knoll et al., 2016). High-resolution analysis needed to support biogenicity.

Age [Ma]	Lithostratigraphic Unit	Paleoenvironment	Morphological Evidence	Geochemical Evidence	Comments
3334 ²	Kromberg Fm. (K3) (Loseisdal Chert)	Nearshore, possibly hydrothermal	Microbial mats: carbonaceous laminae (~10µm thick) in layered packets of 100–1000 µm thickness; eroded fragments of biofilms. (Westall et al., 2001; 2006; 2011; 2015). Putative rod-shaped microfossils are probably abiogenic (Altermann, 2001; Wacey 2009).	<i>Bulk</i> $\delta^{13}C_{org}$: -26.8‰ and -22.7‰ (n=2) <i>In situ</i> : $\delta^{13}C_{org}$: -45‰ to -13‰ $\delta^{34}S$: -2.4‰	Petrographic observations and geochemical signals support the biogenic origin.
3416 ³	Kromberg Fm. (K1) (Buck Reef Chert)	shallow-marine	Microbial mats: fine carbonaceous laminae with different morphotypes, draping underlying sediments and detrital particles; filaments (1–1.5 µm in diameter), rolled-up fragments; carbonaceous grains (Walsh and Lowe, 1999; Tice and Lowe, 2004a, 2006a, b; Tice, 2009; Tice et al., 2011). Probable microfossils: lenticular structures (13–135 µm long and 4.5–61 µm wide) with hollow center, interpreted as remnants of possibly planktonic microbes (Walsh, 1992; Oehler et al., 2017). Similar structures also occur in cherts of the Pilbara Craton. Possible microfossils: filamentous structures (1.2–1.4 µm in diameter), sometimes interwoven clumps spheroidal structures (10–84 µm and 4.5–12.8 µm in diameter) (Walsh and Lowe, 1985; Walsh 1992, 2000)	<i>Bulk</i> $\delta^{13}C_{org}$: -36.9‰ and -20.1‰ (n=19) <i>In situ</i> $\delta^{13}C_{org}$: -39.3‰ to -35.5‰ (n=8) None, except carbonaceous composition	Widespread, well-documented, and morphological complex evidence for life. Depositional context, morphological complexity, and narrow range of $\delta^{13}C_{org}$ values support a biological origin. High-resolution petrographic and <i>in situ</i> carbon isotope analysis needed.
3416 ³	Kromberg Fm. (K1c2) (Buck Reef Chert)	shallow-marine	Possible microfossils: spheroidal (3–12 µm in diameter) interpreted as remains of beuthic-planktonic microbes, resembling coccolidal cyanobacteria (Kremer and Kazmierczak, 2017).	<i>Bulk</i> $\delta^{13}C_{org}$: -26.5‰ and -24.3‰ (n=2)	Morphologically simple structures with angular terminations. Nanoscale analysis and <i>in situ</i> geochemical data needed.
~3450	Kromberg Fm. and Hoogenoeg Fm.	Submarine pillow basalts	Possible trace fossils: filament-shaped and titanite-mineralized microtubes (4 µm in diameter and up to 200µm in length) in glassy pillow lava rims (Furnes et al., 2004). Similarity to microtubes from recent pillow lavas, but even their microbial origin is debated (Wacey et al., 2017).	<i>Bulk</i> $\delta^{13}C_{carb}$: -16.4‰ to +3.9‰ <i>In situ</i> $\delta^{34}S_{CDT}$: -40‰ to -3‰ from pyrite	Syn- and biogenicity questioned by Grosch and McLaughlin (2014) and Grosch et al. (2016), structures likely formed abiotically during post depositional contact metamorphism.
	Hoogenoeg Fm.	?	Possible microfossils: spheroidal and cup-shaped structures; 5–106 µm in diameter (Engel et al., 1968).	None, except carbonaceous composition	Probably of non-biological origin (Nagy and Nagy, 1969; Schopf and Walter, 1983). Promising sign for life, but no geochemical data.
3470 ⁴	Hoogenoeg Fm. (H3c, H5c)	Seafloor, possibly hydrothermal	Possible microfossils: spheroidal structures (2–10 µm in diameter) with granular 'cell' walls interpreted as remnants of chemosynthetic microbes (Glikson et al., 2008). Morphological similarity to modern hyperthermophilic microbes.	None	Promising sign for life, but no geochemical data.
3472 ⁵	Hoogenoeg Fm. Middle Marker (H1)	Shallow marine, associated with volcanic activity	Microbial mats: fine, crinkly to micro-tufted laminations, 'trapped' detrital sediment, wisp-like microstructures interpreted as eroded biofilm or mat fragments (Hickman-Lewis et al., 2018).	None, except carbonaceous composition and REE data	Carbon isotope data needed to further support biogenicity of the possibly most ancient trace of life in the BCB.

Age Dates: ¹Heubbeck et al., 2013 ²Byerly et al., 1999 ³Kröner et al., 1991 ⁴Byerly et al., 1999 ⁵Armstrong et al., 1990